

A registration method for model order reduction: data compression and geometry reduction

Tommaso Taddei¹

¹ IMB, UMR 5251, Univ. Bordeaux; 33400, Talence, France. Inria Bordeaux Sud-Ouest, Team MEMPHIS; 33400, Talence, France,
tommaso.taddei@inria.fr

Abstract

We propose a general — i.e., independent of the underlying equation — registration method for parameterized Model Order Reduction. Given the spatial domain $\Omega \subset \mathbb{R}^d$ and a set of snapshots $\{u^k\}_{k=1}^{n_{\text{train}}}$ over Ω associated with n_{train} values of the model parameters $\mu^1, \dots, \mu^{n_{\text{train}}} \in \mathcal{P}$, the algorithm returns a parameter-dependent bijective mapping $\Phi : \Omega \times \mathcal{P} \rightarrow \mathbb{R}^d$: the mapping is designed to make the mapped manifold $\{u_\mu \circ \Phi_\mu : \mu \in \mathcal{P}\}$ more suited for linear compression methods. We apply the registration procedure, in combination with a linear compression method, to devise low-dimensional representations of solution manifolds with slowly-decaying Kolmogorov N -widths; we also consider the application to problems in parameterized geometries. We present a theoretical result to show the mathematical rigor of the registration procedure. We further present numerical results for several two-dimensional problems, to empirically demonstrate the effectivity of our proposal.

Keywords: parameterized partial differential equations; model order reduction; data compression; geometry registration.

1 Introduction

1.1 Background

Numerical simulations based on mathematical models represent a valuable tool to study complex phenomena of scientific interest and/or industrial value. For several applications — including design and optimization, uncertainty quantification, active control — it is important to approximate the solution (and associated quantities of interest) to the model over a range of parameters: parameters might correspond to material properties, geometric features, operating conditions. To alleviate the computational burden associated with the evaluation of the model for many values of the parameters, parameterized Model Order Reduction (pMOR) techniques aim to generate a Reduced Order Model (ROM) that approximates the original system over a prescribed parameter range. In this work, we shall develop a *general* — i.e., independent of the underlying equation — registration procedure for pMOR applications; we shall here focus on systems modelled by stationary Partial Differential Equations (PDEs).

We denote by μ the set of parameters associated with the model in the prescribed parameter domain $\mathcal{P} \subset \mathbb{R}^P$; we denote by $\Omega \subset \mathbb{R}^d$ ($d = 2, 3$) the

spatial domain, which is assumed to be Lipschitz; we also introduce the Hilbert space \mathcal{X} defined over Ω , endowed with the inner product (\cdot, \cdot) and the induced norm $\|\cdot\| := \sqrt{(\cdot, \cdot)}$. Then, we introduce the problem:

$$\text{find } \mathbf{y}_\mu := \mathbf{s}_\mu(z_\mu) \text{ s.t. } \mathcal{G}_\mu(z_\mu, v) = 0 \quad \forall v \in \mathcal{X}, \quad (1)$$

where \mathbf{y}_μ is a vector of D quantities of interest, $\mathbf{s}_\mu : \mathcal{X} \rightarrow \mathbb{R}^D$ is a continuous functional, and $\mathcal{G}_\mu(z_\mu, \cdot) = 0$ admits a unique solution for all $\mu \in \mathcal{P}$. We denote by $\mathcal{M} := \{z_\mu : \mu \in \mathcal{P}\} \subset \mathcal{X}$ the solution manifold associated with the parametric problem, and we denote by \tilde{z}_μ the approximation to z_μ provided by a given ROM, for $\mu \in \mathcal{P}$.

A pMOR technique for (1) relies on three building blocks: (i) a data compression strategy for the construction of a low-dimensional approximation space of the solution manifold \mathcal{M} ; (ii) a reduced-order statement for the rapid and reliable prediction of the solution and associated quantities of interest for any value of the parameter; and (iii) an *a posteriori* error estimation procedure for certification. pMOR strategies rely on an *offline/online* computational decomposition: during the offline stage, which is computationally expensive and performed once, a ROM for (1) is generated by exploiting several high-fidelity (Finite Element, Finite Volume,...) solutions to the mathematical model for (properly-chosen) parameter values; during the online stage, which is inexpensive and performed for any new parameter value μ , the solution to the ROM is computed to rapidly obtain predictions of z_μ and associated quantities of interest. In the past few decades, many authors have developed pMOR strategies for a broad class of problems: we refer to the surveys [5, 22, 46] for thorough introductions to pMOR.

In (1), we assume that the domain Ω is fixed (parameter-independent); however, for several applications, the problem of interest is of the form:

$$\text{find } \mathbf{y}_\mu := \mathbf{s}_\mu(z_\mu) \text{ s.t. } \mathcal{G}_\mu(z_\mu, v) = 0 \quad \forall v \in \mathcal{X}_\mu, \quad (2)$$

where \mathcal{X}_μ is a suitable Hilbert space defined over the parameter-dependent domain $\Omega_\mu \subset \mathbb{R}^d$. Note that solution fields for different parameters are defined over different spatial domains: hence it is not possible to combine solutions to the parameterized model for different parameter values. The latter prevents the direct application of pMOR techniques to (2).

Parametric mappings are used in pMOR to recast problem (1) or (2) as

$$\text{find } \mathbf{y}_\mu := \mathbf{s}_{\mu, \Phi}(\tilde{z}_\mu) \text{ s.t. } \mathcal{G}_{\mu, \Phi}(\tilde{z}_\mu, v) = 0 \quad \forall v \in \mathcal{X}, \quad (3)$$

where $\mathbf{s}_{\mu, \Phi}(w) := \mathbf{s}_\mu(w \circ \Phi_\mu^{-1})$, and $\mathcal{G}_{\mu, \Phi}(w, v) := \mathcal{G}_\mu(w \circ \Phi_\mu^{-1}, v \circ \Phi_\mu^{-1})$ for all $w, v \in \mathcal{X}$. We denote by $\tilde{\mathcal{M}} := \{\tilde{z}_\mu = z_\mu \circ \Phi_\mu : \mu \in \mathcal{P}\}$ the mapped solution manifold. For (1), we require that Φ_μ is a bijection from Ω into itself, for all $\mu \in \mathcal{P}$; furthermore, we require that $v \circ \Phi_\mu^{-1} \in \mathcal{X}$ for all $v \in \mathcal{X}$. For (2), we require that Φ_μ is a bijection from a reference domain Ω into Ω_μ and that $\mathcal{G}_{\mu, \Phi}$ is well-posed in $\mathcal{X} := \{v \circ \Phi_\mu : v \in \mathcal{X}_\mu\}$. Note that in (1) mappings are employed to obtain a more efficient (lower-dimensional) representation of the solution manifold; on the other hand, in (2), mappings are introduced to recast the problem in a form that allows the application of pMOR techniques.

Problem-dependent mappings are broadly used in Applied Mathematics to compress information and ultimately simplify the solution to PDEs. r -adaptivity

([60]) is used in combination with DG discretization methods to approximate discontinuous solutions to hyperbolic PDEs; similarly, problem-dependent scaling factors — in effect, mappings — are used to determine self-similar (approximate) solutions to PDEs, including the boundary layer equations (see, e.g., [40, Chapter 16.4]). Furthermore, problem-dependent mappings are employed to devise high-fidelity solvers for problems in deforming domains ([16, 43]). We describe below the two classes of pMOR tasks considered in this work.

1.2 Data compression of problems with slowly-decaying Kolmogorov widths

Most approaches to data compression for (1) rely on linear approximation spaces $\mathcal{Z}_N = \text{span}\{\zeta_n\}_{n=1}^N \subset \mathcal{X}$ to approximate the manifold \mathcal{M} : we refer to this class of methods as to *linear approximation (or compression) methods*; given \mathcal{Z}_N , we denote by $Z_N : \mathbb{R}^N \rightarrow \mathcal{Z}_N$ the linear parameter-independent operator such that $Z_N \boldsymbol{\alpha} := \sum_{n=1}^N \alpha_n \zeta_n$, for all $\boldsymbol{\alpha} \in \mathbb{R}^N$. Two well-known linear approximation methods are the Proper Orthogonal Decomposition (POD, [7, 51, 57]) and the weak-Greedy algorithm ([50, section 7.2.2]). Success of linear methods relies on the availability of low-dimensional accurate approximation spaces for the solution manifold \mathcal{M} . The Kolmogorov N -width ([44]) provides a rigorous measure of the linear reducibility of \mathcal{M} : given $N > 0$, the Kolmogorov N -width $d_N(\mathcal{M})$ is given by

$$d_N(\mathcal{M}) := \inf_{\mathcal{Z}_N \subset \mathcal{X}, \dim(\mathcal{Z}_N)=N} \sup_{w \in \mathcal{M}} \|w - \Pi_{\mathcal{Z}_N} w\|, \quad (4)$$

where the infimum is taken over all N -dimensional spaces, and $\Pi_{\mathcal{Z}_N} : \mathcal{X} \rightarrow \mathcal{Z}_N$ denotes the orthogonal projection operator onto $\mathcal{Z}_N \subset \mathcal{X}$. In certain engineering-relevant cases, it is possible to demonstrate that the decay of $d_N(\mathcal{M})$ with N is extremely rapid: we refer to [50, section 8.1], [2, Theorem 3.3] and [13, 14] for further details. Recalling the (quasi-)optimality properties of POD and Greedy algorithms (see [57] and [13], respectively), rapid-decaying Kolmogorov widths justify the use of linear methods.

However, linear approximation methods are fundamentally ill-suited for several classes of relevant engineering problems. As observed in [21, Example 3.5] and [54, Example 2.5], solution fields with parameter-dependent jump discontinuities — or alternatively boundary/internal layers — cannot be adequately approximated through a low-dimensional linear expansion; similarly, linear methods are inappropriate to deal with problems with discontinuous parameter-dependent coefficients. Motivated by these considerations, several authors have proposed *nonlinear approximation/compression methods* to deal with these problems: we here distinguish between *Eulerian* and *Lagrangian* approaches.

Eulerian approaches consider approximations of the form $\hat{z}_\mu := Z_{N,\mu}(\hat{\boldsymbol{\alpha}}_\mu)$, where $Z_{N,\mu} : \mathbb{R}^N \rightarrow \mathcal{X}$ is a suitably-chosen operator which might depend on the parameter μ and might also be nonlinear in $\boldsymbol{\alpha}$. Eulerian techniques might rely on Grassmannian learning [1, 61], convolutional auto-encoders [25, 27], transported/transformed snapshot methods [10, 35, 47, 58], displacement interpolation [48], to determine the operator $Z_{N,\mu}$. Alternatively, they might exploit adaptive local-in-parameter and/or local-in-space enrichment strategies [3, 6, 11, 17, 18, 19, 39, 41]. Note that, since $Z_{N,\mu}$ is nonlinear and/or depends

on parameter, it might be difficult to develop rapid and reliable procedures for the online computations of the coefficients $\hat{\alpha}_\mu$.

Lagrangian approaches propose to exploit a linear method $\tilde{Z}_N : \mathbb{R}^N \rightarrow \tilde{\mathcal{Z}}_N \subset \mathcal{X}$ to approximate the mapped solution $\tilde{z}_\mu := z_\mu \circ \Phi_\mu$ where $\Phi_\mu : \Omega \rightarrow \Omega$ is a suitably-chosen bijection from Ω into itself: the mapping Φ_μ should be chosen to make the mapped solution manifold $\tilde{\mathcal{M}}$ more amenable for linear approximations. Examples of Lagrangian approaches have been proposed in¹ [24, 34, 37, 54]: in [37, 54] the construction of the map is performed separately from the construction of the solution coefficients, while in [34] the authors propose to build the mapping Φ_μ and the solution coefficients $\hat{\alpha}_\mu$ simultaneously. Note that Lagrangian approaches are significantly less general than Eulerian approaches — any Lagrangian method is equivalent to an Eulerian method with $Z_{N,\mu}(\alpha) := \sum_{n=1}^N \alpha_n \tilde{z}_n \circ \Phi_\mu^{-1}$ — and thus potentially less powerful in terms of approximation. On the other hand, the application of pMOR techniques to the mapped problem (3) is completely standard: this is in contrast with Eulerian approaches, which might require more involved strategies for the computation of the solution coefficients $\hat{\alpha}_\mu$ (see [27]).

1.3 Reduction of problems in parameterized domains

Given the family of parameterized domains $\{\Omega_\mu : \mu \in \mathcal{P}\}$, we shall here identify a reference domain Ω and a bijective mapping Φ such that $\Omega_\mu = \Phi_\mu(\Omega)$ for all $\mu \in \mathcal{P}$; the mapping should be computable for new values of $\mu \in \mathcal{P}$, with limited computational and memory resources. Several authors have developed geometry reduction techniques based on automatic piecewise-affine maps ([50]), Radial Basis Functions ([31]), transfinite maps ([28, 23]) and solid extension ([30]). While the approach in [50] is restricted to a specific class of parametric deformations, the other approaches — which exploit ideas originally developed in the framework of mesh deformation and surface interpolation/approximation — are broadly applicable. Despite the many recent contributions to the field, development of rapid and reliable geometry reduction techniques for large deformations is still a challenging task.

For applications to biological systems, parametric descriptions of the boundary $\partial\Omega_\mu$ for all μ are unavailable. For this reason, in order to find the mapping Φ , it is important to implement strategies to systematically determine parametric descriptions of $\partial\Omega_\mu$. This problem, which is shared by many of the geometry reduction approaches mentioned above, is not addressed in the present paper.

1.4 Contributions and outline of the paper

We propose a registration procedure that takes as input a set of snapshots $\{u^k = u_{\mu^k}\}_{k=1}^{n_{\text{train}}} \subset L^2(\Omega)$ with $\mu^1, \dots, \mu^{n_{\text{train}}} \in \mathcal{P}$, and returns the parametric mapping $\{\Phi_\mu : \mu \in \mathcal{P}\}$. The key features of the approach are (i) a nonlinear non-convex optimization statement that aims at reducing the difference (in a suitable metric) between a properly-chosen reference field $\bar{u} = u_{\bar{\mu}}$ and the mapped field $\tilde{u}_{\mu^k} = u_{\mu^k} \circ \Phi_{\mu^k}$ for $\mu^1, \dots, \mu^{n_{\text{train}}}$, and (ii) a generalization procedure based on

¹ The method of freezing proposed in [37] aims at decomposing the solution into a group component and a shape component. The approach reduces to a Lagrangian approach if the group action is induced by a mapping of the underlying spatial domain.

Kernel regression that aims at determining a mapping for all $\mu \in \mathcal{P}$ based on the available data for $\{\mu^k\}_{k=1}^{n_{\text{train}}}$.

For nonlinear data compression, we apply the registration procedure to the solution itself ($u_\mu = z_\mu$) or to selected coefficients of the PDE model; for geometry reduction, we should consider $u_\mu = \mathbb{1}_{\Omega_\mu}$ with $\bar{u} = \mathbb{1}_\Omega$, where $\mathbb{1}_A$ is the indicator function of the set $A \subset \mathbb{R}^d$. To demonstrate the generality of the approach for data compression, we consider the application to a boundary layer problem and to an advection-reaction problem with a parameter-dependent sharp gradient region; on the other hand, we consider the application to two diffusion problems to demonstrate the effectivity of our proposal to geometry reduction.

We observe that the present paper is related to a number of prior works. First, as the Eulerian approach in [27], our registration algorithm is independent of the underlying equation: for this reason, we believe that the approach can be applied to a broad class of problems in science and engineering. Second, our optimization statement for the construction of Φ_μ is related to the recent proposal by Zahr and Persson for r -adaptivity in the DG framework ([60]). Third, the optimization statement is tightly linked to optimal transport ([56]), which has been employed in [24] to devise a nonlinear approximation method: in section 2.2.3, we discuss similarities and differences between the mappings obtained using our method and optimal transport maps.

The outline of the paper is as follows. In section 2, we present the registration procedure. Then, in sections 3 and 4, we discuss the application to data compression and geometry reduction; for each task, we investigate performance through the vehicle of two model problems. Finally, in section 5, we provide a short summary and we discuss several potential next steps.

2 Registration procedure

Let \mathcal{U} be a Banach space defined over Ω and contained in $L^2(\Omega)$, and let $\mathcal{M}_u := \{u_\mu : \mu \in \mathcal{P}\} \subset \mathcal{U}$ be a suitable parametric manifold: as discussed in the introduction, u_μ might be the solution to a parameterized PDE, a (set of) coefficient(s) associated with a PDE model \mathcal{G}_μ , or the indicator function associated with a family of parameterized domains. In this work, we assume that u_μ is scalar: nevertheless, we envision that the approach can be extended to vector-valued fields with only minor modifications. The goal of this section is to develop a computational procedure that takes as input snapshots of \mathcal{M}_u , $\{u^k = u_{\mu^k}\}_{k=1}^{n_{\text{train}}}$, and returns a parametric mapping $\{\Phi_\mu : \mu \in \mathcal{P}\}$ from Ω into itself. We defer to sections 3 and 4 the discussion about the practical application of the present framework to the two pMOR tasks of interest.

It is important to clarify the desiderata for Φ_μ . First, since we are ultimately interested in estimating the mapped solution $\tilde{z}_\mu := z_\mu \circ \Phi_\mu^{-1}$, the mapping should satisfy

$$\Phi_\mu(\Omega) = \Omega, \quad \text{such that } \mathfrak{J}_\mu(\mathbf{X}) := \det(\hat{\nabla} \Phi_\mu(\mathbf{X})) \in \left[\epsilon, \frac{1}{\epsilon} \right] \quad \forall \mathbf{X} \in \bar{\Omega}, \quad (5)$$

for all $\mu \in \mathcal{P}$, where $\epsilon > 0$ is a prescribed tolerance that bounds the maximum allowed pointwise contraction induced by the mapping and its inverse, and $\hat{\nabla} =$

$[\hat{\partial}_1, \dots, \hat{\partial}_d]$ denotes the gradient with respect to the reference configuration. We also require that Φ_μ is sufficiently smooth to satisfy

$$v \in \mathcal{X} \Leftrightarrow v \circ \Phi_\mu^{-1} \in \mathcal{X} \quad \forall \mu \in \mathcal{P}. \quad (6)$$

If \mathcal{X} is either $L^2(\Omega)$ or $H^1(\Omega)$, it suffices to require that Φ_μ and its inverse are Lipschitz continuous for all $\mu \in \mathcal{P}$. Second, for any given $N > 0$, we shall design Φ_μ such that

$$d_N(\widetilde{\mathcal{M}}_u) \ll d_N(\mathcal{M}_u), \quad \text{where } \widetilde{\mathcal{M}}_u := \{u_\mu \circ \Phi_\mu : \mu \in \mathcal{P}\}. \quad (7)$$

Here, d_N is the Kolmogorov N -width (4) of the manifold $\widetilde{\mathcal{M}}_u$.

In this work, we seek mappings of the form

$$\Phi_\mu(\mathbf{X}) := \mathbf{X} + \sum_{m=1}^M (\hat{\mathbf{a}}_\mu)_m \varphi_m(\mathbf{X}), \quad (8)$$

where $\hat{\mathbf{a}} : \mathcal{P} \rightarrow \mathbb{R}^M$ is a vector-valued function of the parameters, and $\{\varphi_m\}_{m=1}^M \subset \text{Lip}(\Omega; \mathbb{R}^d)$ is a set of properly-defined functions, which are linear combinations of a larger set of functions $\{\varphi_m^{\text{hf}}\}_{m=1}^{M_{\text{hf}}} \subset \text{Lip}(\Omega; \mathbb{R}^d)$. In view of the presentation of the algorithm, it is convenient to introduce the parametric function $\{\Psi_{\mathbf{a}}^{\text{hf}} : \Omega \rightarrow \mathbb{R}^d\}_{\mathbf{a} \in \mathbb{R}^{M_{\text{hf}}}}$ such that $\Psi_{\mathbf{a}}^{\text{hf}}(\mathbf{X}) := \mathbf{X} + \sum_{m=1}^{M_{\text{hf}}} a_m \varphi_m^{\text{hf}}(\mathbf{X})$: Ψ^{hf} is used at training stage to generate the problem-dependent mapping Φ_μ . Clearly, the choice of Ψ^{hf} should depend on the particular domain Ω considered. Given a set of functions $\{\varphi_m^{\text{hf}}\}_{m=1}^{M_{\text{hf}}}$, we define

$$A_{\varphi, \epsilon}^{\text{hf}} := \left\{ \mathbf{a} \in \mathbb{R}^{M_{\text{hf}}} : \Phi = \mathbf{X} + \sum_m a_m \varphi_m^{\text{hf}}(\mathbf{X}) \text{ satisfies (5)} \right\}. \quad (9)$$

Clearly, $\mathbf{0} \in A_{\varphi, \epsilon}^{\text{hf}}$ for any choice of $\{\varphi_m^{\text{hf}}\}_{m=1}^M$ and $\epsilon \in (0, 1)$; in section 2.1 (cf. Lemma 2.1), we prove that, under certain conditions on the functions $\{\varphi_m^{\text{hf}}\}_{m=1}^{M_{\text{hf}}}$, there exists a non-trivial neighborhood of $\mathbf{a} = \mathbf{0}$ that is contained in $A_{\varphi, \epsilon}^{\text{hf}}$.

Algorithm 1 summarizes the pieces of the general approach proposed in this paper. Note that the algorithm takes as input a reference parameter $\bar{\mu} \in \mathcal{P}$. In the remainder of this section, we discuss each step of the procedure separately: in section 2.1, we discuss how to choose the parametric function $\{\Psi_{\mathbf{a}}^{\text{hf}} : \Omega \rightarrow \mathbb{R}^d\}_{\mathbf{a} \in \mathbb{R}^{M_{\text{hf}}}}$; in section 2.2, we introduce and motivate the optimization problem employed to choose \mathbf{a}_{hf}^k associated with the k -th snapshot and \bar{u} , for $k = 1, \dots, n_{\text{train}}$; in section 2.3, we discuss generalization, that is how to exploit the dataset $\{(\mu^k, \mathbf{a}_{\text{hf}}^k)\}_{k=1}^{n_{\text{train}}}$ to define the vector-valued function $\hat{\mathbf{a}} : \mathcal{P} \rightarrow \mathbb{R}^M$.

Algorithm 1 Registration algorithm

Inputs: $\{u^k = u_{\mu^k}\}_{k=1}^{n_{\text{train}}} \subset \mathcal{U}$ snapshot set, $\bar{\mu} \in \mathcal{P}$ reference parameter.

Output: $\hat{\mathbf{a}} : \mathcal{P} \rightarrow \mathbb{R}^M$, $\{\varphi_m\}_{m=1}^M$, parametric mapping (cf. (8)).

- 1: Definition of the parametric function $\{\Psi_{\mathbf{a}}^{\text{hf}} : \Omega \rightarrow \mathbb{R}^d\}_{\mathbf{a} \in \mathbb{R}^{M_{\text{hf}}}}$
- 2: Computation of \mathbf{a}_{hf}^k based on the pair of fields $(u^k, \bar{u} := u_{\bar{\mu}}) \rightarrow \{(\mu^k, \mathbf{a}_{\text{hf}}^k)\}_{k=1}^{n_{\text{train}}}$
- 3: Generalization: $\{(\mu^k, \mathbf{a}_{\text{hf}}^k)\}_{k=1}^{n_{\text{train}}} \rightarrow \hat{\mathbf{a}} : \mathcal{P} \rightarrow \mathbb{R}^M$, $\{\varphi_m\}_{m=1}^M$
- 4: Return $\{\Phi_\mu(\mathbf{X}) := \mathbf{X} + \sum_{m=1}^M (\hat{\mathbf{a}}_\mu)_m \varphi_m(\mathbf{X}) : \mu \in \mathcal{P}\}$.

2.1 Parameterization

2.1.1 Theoretical preliminaries

We state in Proposition 2.1 a theoretical result that is used in section 2.1.2 to choose the parametric function $\{\Psi_{\mathbf{a}}^{\text{hf}}\}_{\mathbf{a}}$. Proof of Proposition 2.1 is provided in Appendix B. We say that $U \subset \mathbb{R}^d$ is diffeomorphic to $V \subset \mathbb{R}^d$ (and we use notation $U \simeq V$) if there exists a differentiable function \mathbf{H} with differentiable inverse such that $\mathbf{H}(U) = V$. Given $\delta > 0$, we denote by Ω_δ the δ -neighbourhood of Ω , $\Omega_\delta := \{\mathbf{x} \in \mathbb{R}^d : \text{dist}(\mathbf{x}, \Omega) < \delta\}$.

Proposition 2.1. *Let $\Omega \subset \mathbb{R}^d$ satisfy*

$$\Omega \simeq \widehat{\Omega} = \{\mathbf{x} \in \mathbb{R}^d : f(\mathbf{x}) < 0\}, \quad \text{where } f : \mathbb{R}^d \rightarrow \mathbb{R} \text{ is convex.} \quad (10)$$

Given $\delta > 0$, let $\Phi : \Omega_\delta \rightarrow \mathbb{R}^d$ be a vector-valued function that satisfies

$$(i) \quad \Phi \in C^1(\Omega_\delta; \mathbb{R}^d);$$

$$(ii) \quad \mathfrak{J}(\mathbf{X}) := \det(\widehat{\nabla} \Phi(\mathbf{X})) \geq \epsilon > 0 \text{ for all } \mathbf{X} \in \Omega \text{ and a given } \epsilon > 0;$$

$$(iii) \quad \text{dist}(\Phi(\mathbf{X}), \partial\Omega) = 0 \text{ for all } \mathbf{X} \in \partial\Omega \text{ (i.e., } \Phi(\partial\Omega) \subseteq \partial\Omega).$$

Then, Φ is a bijection that maps Ω into itself.

We observe that the (unit) ball and the (unit) hyper-cube satisfy (10): we have indeed that $\mathcal{B}_1(\mathbf{0}) = \{\mathbf{x} \in \mathbb{R}^d : f(\mathbf{x}) = \|\mathbf{x}\|_2^2 - 1 < 0\}$, and $(0, 1)^d = \{\mathbf{x} \in \mathbb{R}^d : f(\mathbf{x}) = 2\|\mathbf{x} - [1/2, 1/2]\|_\infty - 1 < 0\}$. We further observe that, if Ω satisfies (10), so does any domain diffeomorphic to Ω . Finally, we remark that $\partial\widehat{\Omega} = \{\mathbf{x} \in \mathbb{R}^d : f(\mathbf{x}) = 0\}$: this implies that any Ω satisfying (10) is simply connected with connected boundary. Note that any simply-connected two-dimensional Lipschitz domain satisfies (10); the latter result is in general false for $d = 3$.

Figure 1 provides a geometric interpretation of conditions (i) and (iii) in Proposition 2.1 for the unit square $\Omega = (0, 1)^2$: if $\mathbf{X} \in \partial\Omega$, $\Phi(\mathbf{X})$ is constrained to belong to the boundary $\partial\Omega$; furthermore, since $\Phi \in C^1$, corners of Ω should be mapped in themselves, that is $\Phi(\{(0, 0), (1, 0), (0, 1), (1, 1)\}) = \{(0, 0), (1, 0), (0, 1), (1, 1)\}$. As a result, up to a rotation, all edges of the unit square should be mapped in themselves.

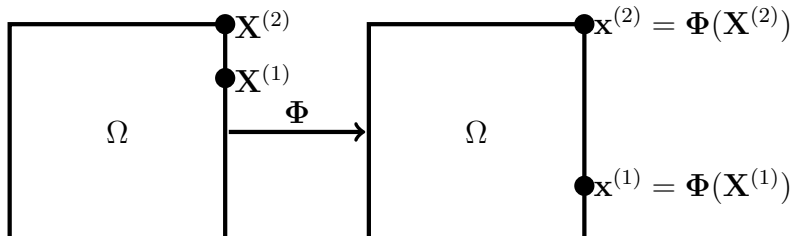


Figure 1: geometric interpretation of the conditions (i) and (iii) in Proposition 2.1.

Corollary 2.2 illustrates an extension of Proposition 2.1 to a broader class of domains.

Corollary 2.2. Let $\Omega = \Omega^{\text{out}} \setminus \bigcup_{i=1}^Q \Omega_i^{\text{in}}$. Let $\Omega^{\text{out}}, \Omega_1^{\text{in}}, \dots, \Omega_Q^{\text{in}} \subset \mathbb{R}^d$ satisfy the following assumptions.

- (i) $\Omega_1^{\text{in}}, \dots, \Omega_Q^{\text{in}}, \Omega^{\text{out}}$ satisfy (10).
- (ii) $\Omega_1^{\text{in}}, \dots, \Omega_Q^{\text{in}}$ are pairwise disjoint, and $\Omega_1^{\text{in}}, \dots, \Omega_Q^{\text{in}} \subset \subset \Omega^{\text{out}}$.

Let $\Phi : \Omega_\delta^{\text{out}} \rightarrow \mathbb{R}^d$ be a function such that

- (i) $\Phi \in C^1(\Omega_\delta^{\text{out}}; \mathbb{R}^d)$;
- (ii) $\mathfrak{J}(\mathbf{X}) \geq \epsilon > 0$ for all $\mathbf{X} \in \Omega^{\text{out}}$ and a given $\epsilon > 0$;
- (iii) $\Phi(\partial\Omega^{\text{out}}) \subseteq \partial\Omega^{\text{out}}$, $\Phi(\partial\Omega_i^{\text{in}}) \subseteq \partial\Omega_i^{\text{in}}$ for $i = 1, \dots, Q$.

Then, Φ is a bijection that maps Ω into itself.

Proof. We first observe that, by construction, we have $\partial\Omega = \partial\Omega^{\text{out}} \cup \bigcup_{i=1}^Q \partial\Omega_i^{\text{in}}$. Exploiting Proposition 2.1, we find that Φ is a bijection that maps $\Omega^{\text{out}}, \Omega_1^{\text{in}}, \dots, \Omega_Q^{\text{in}}$ into themselves. Then, we observe that

$$\Phi(\Omega) = \Phi \left(\Omega^{\text{out}} \setminus \bigcup_{i=1}^Q \Omega_i^{\text{in}} \right) = \Phi(\Omega^{\text{out}}) \setminus \bigcup_{i=1}^Q \Phi(\Omega_i^{\text{in}}) = \Omega^{\text{out}} \setminus \bigcup_{i=1}^Q \Omega_i^{\text{in}} = \Omega.$$

Thesis follows. \square

2.1.2 Choice of Ψ^{hf} for $\Omega = (0, 1)^2$

We shall now discuss how to exploit the results of section 2.1.1 to choose the parameterized function Ψ^{hf} . We here tailor our discussion to $\Omega = (0, 1)^2$, which is the domain considered, up to a scaling factor, in all the numerical examples of this paper: we refer to a future work for the extension to other choices of Ω . In the next Lemma, we introduce the parameterization considered in this work.

Lemma 2.1. Let $\{\Psi_{\mathbf{a}}^{\text{hf}}\}_{\mathbf{a}}$ be of the form

$$\Psi_{\mathbf{a}}^{\text{hf}}(\mathbf{X}) := \mathbf{X} + \sum_{m=1}^{M_{\text{hf}}} a_m \varphi_m^{\text{hf}}(\mathbf{X}), \quad \mathbf{X} \in \Omega, \quad \mathbf{a} = [a_1, \dots, a_{M_{\text{hf}}}]^T \in \mathbb{R}^{M_{\text{hf}}}, \quad (11a)$$

where $\{\varphi_m^{\text{hf}}\}_{m=1}^{M_{\text{hf}}} \subset C^1(\mathbb{R}^2; \mathbb{R}^2)$ satisfy

$$\begin{cases} \varphi_m^{\text{hf}}(\mathbf{X}) \cdot \mathbf{e}_1 = 0 & \text{on } \{\mathbf{X} : X_1 = 0, \text{ or } X_1 = 1\}, \\ \varphi_m^{\text{hf}}(\mathbf{X}) \cdot \mathbf{e}_2 = 0 & \text{on } \{\mathbf{X} : X_2 = 0, \text{ or } X_2 = 1\}, \end{cases} \quad m = 1, \dots, M_{\text{hf}}. \quad (11b)$$

Here, $\mathbf{e}_1, \mathbf{e}_2$ are the canonical basis of \mathbb{R}^2 . Then, for any $\bar{\mathbf{a}} \in \mathbb{R}^{M_{\text{hf}}}$, $\Phi := \Psi_{\bar{\mathbf{a}}}^{\text{hf}}$ is bijective from Ω into itself if

$$\min_{\mathbf{X} \in \Omega} \mathfrak{J}(\mathbf{X}) := \det(\widehat{\nabla} \Phi(\mathbf{X})) > 0. \quad (12)$$

Furthermore, for any $\epsilon > 0$, there exists a ball of radius $r_\epsilon > 0$ centered in $\mathbf{a} = \mathbf{0}$ that is strictly contained in $A_{\varphi, \epsilon}^{\text{hf}}$ defined in (9).

Proof. Recalling Proposition 2.1, we only need to verify that $\Phi(\partial\Omega) \subset \partial\Omega$. We here verify that $\Phi(\mathcal{E}_{\text{top}}) \subset \mathcal{E}_{\text{top}}$ where $\mathcal{E}_{\text{top}} := \{\mathbf{X} = (t, 1) : t \in (0, 1)\}$ is the top edge of $(0, 1)^2$: proofs for the other edges are analogous.

Exploiting (11b), we have that

$$\Phi(\mathbf{X} = (t, 1)) = \begin{bmatrix} \varphi(t) \\ 1 \end{bmatrix}, \quad \text{where } \varphi(t) := \mathbf{e}_1 \cdot \Phi(\mathbf{X} = (t, 1)).$$

By contradiction, we assume that $\varphi([0, 1])$ is not contained in $[0, 1]$. Since $\varphi(0) = 0$ and $\varphi(1) = 1$, φ has a local minimum or maximum in $(0, 1)$; this implies that there exists $\bar{t} \in (0, 1)$ such that $\varphi'(\bar{t}) = 0$. As a result, we find

$$\mathbf{e}_1^T \widehat{\nabla} \Phi|_{\mathbf{X} = (\bar{t}, 1)} = [\varphi'(\bar{t}), 0] = 0,$$

which implies that $\mathfrak{J}(\mathbf{X} = (\bar{t}, 1)) = 0$. Contradiction.

Proof of the latter statement is a direct consequence of the fact that the determinant of a matrix-valued function is continuous and that $\mathfrak{J}_{\mathbf{a}} \equiv 1$ for $\mathbf{a} = \mathbf{0}$. We omit the details. \square

Lemma 2.1 shows that, if Ψ^{hf} is of the form (11), bijectivity in Ω directly follows from (12): the latter condition is (weakly) imposed in the optimization statement of section 2.2. In our implementation, we define $\varphi_1^{\text{hf}}, \dots, \varphi_{M_{\text{hf}}}^{\text{hf}}$ as follows:

$$\begin{cases} \varphi_{m=i+(i'-1)\bar{M}}^{\text{hf}}(\mathbf{X}) = \ell_i(X_1)\ell_{i'}(X_2)X_1(1-X_1)\mathbf{e}_1 \\ \varphi_{m=\bar{M}^2+i+(i'-1)\bar{M}}^{\text{hf}}(\mathbf{X}) = \ell_i(X_1)\ell_{i'}(X_2)X_2(1-X_2)\mathbf{e}_2 \end{cases} \quad i, i' = 1, \dots, \bar{M}, \quad (13)$$

where $\{\ell_i\}_{i=1}^{\bar{M}}$ are the first \bar{M} Legendre polynomials and $M_{\text{hf}} = 2\bar{M}^2$. Note that $\varphi_1^{\text{hf}}, \dots, \varphi_{M_{\text{hf}}}^{\text{hf}}$ satisfy the boundary conditions in (11b). We emphasize that other choices satisfying (11b) (e.g., Fourier expansions) might also be considered.

2.2 Optimization statement

Given the fields $u^k = u_{\mu^k}, \bar{u} = u_{\bar{\mu}} \in \mathcal{U}$ for $k \in \{1, \dots, n_{\text{train}}\}$, and the parameterization $\{\Psi_{\mathbf{a}}^{\text{hf}}\}_{\mathbf{a}}$, we propose to choose $\mathbf{a}_{\text{hf}}^k = \mathbf{a}_{\text{hf}, \mu^k}$ as a solution to

$$\begin{aligned} & \min_{\mathbf{a} \in \mathbb{R}^{M_{\text{hf}}}} \mathfrak{f}(\mathbf{a}, \mu^k, \bar{\mu}) + \xi |\Psi_{\mathbf{a}}^{\text{hf}}|_{H^2(\Omega)}^2, \\ & \text{s.t. } \int_{\Omega} \exp\left(\frac{\epsilon - \mathfrak{J}_{\mathbf{a}}^{\text{hf}}(\mathbf{X})}{C_{\text{exp}}}\right) + \exp\left(\frac{\mathfrak{J}_{\mathbf{a}}^{\text{hf}}(\mathbf{X}) - 1/\epsilon}{C_{\text{exp}}}\right) dX \leq \delta, \end{aligned} \quad (14a)$$

where $\mathfrak{J}_{\mathbf{a}}^{\text{hf}} = \det(\widehat{\nabla} \Psi_{\mathbf{a}}^{\text{hf}})$. Here, \mathfrak{f} is a measure of the proximity of $u^k \circ \Psi_{\mathbf{a}}^{\text{hf}}$ to \bar{u} , which is introduced below. The Tikhonov-type penalty term $\xi |\Psi_{\mathbf{a}}^{\text{hf}}|_{H^2(\Omega)}^2$ is designed to bound second-order derivatives of the mapping². Note that $|\Psi_{\mathbf{a}=\mathbf{0}}^{\text{hf}}|_{H^2(\Omega)}^2 = 0$: the penalty term thus measures deviations from the identity map. Finally, the nonlinear constraint imposes weakly that the Jacobian determinant $\mathfrak{J}_{\mathbf{a}}^{\text{hf}}(\mathbf{X})$ belongs to the box $[\epsilon, 1/\epsilon]$ for all $\mathbf{X} \in \Omega$.

² Recall that $|v|_{H^2(\Omega)}^2 := \sum_{i,j,k=1}^d \int_{\Omega} \left(\widehat{\partial}_{i,j}^2 v_k\right)^2 dX$ for all $v \in H^2(\Omega; \mathbb{R}^d)$.

Statement (14a) depends on four hyper-parameters: $\xi, \epsilon, C_{\text{exp}}, \delta$. The regularization parameter $\xi > 0$ balances accuracy — measured by \mathfrak{f} — and smoothness of the mapping; the positive constant $\epsilon \in (0, 1)$ can be interpreted as the maximum allowed pointwise contraction induced by the mapping Ψ^{hf} and by its inverse; the scaling factor C_{exp} should be significantly smaller than ϵ to ensure that $\min_{\mathbf{X}} \mathfrak{J}_{\mathbf{a}}(\mathbf{X}) \gtrsim \epsilon$ for all \mathbf{a} satisfying the constraint; finally, δ should satisfy

$$\delta \geq |\Omega| \left(\exp\left(\frac{\epsilon - 1}{C_{\text{exp}}}\right) + \exp\left(\frac{1 - 1/\epsilon}{C_{\text{exp}}}\right) \right),$$

so that $\mathbf{a} = \mathbf{0}$ is admissible. In all our numerical examples, we choose

$$C_{\text{exp}} = 0.025\epsilon, \quad \delta = |\Omega|. \quad (14b)$$

2.2.1 Choice of the proximity measure

A natural choice for \mathfrak{f} , which is considered in the examples of section 3, is

$$\mathfrak{f}(\mathbf{a}, \mu, \bar{\mu}) := \int_{\Omega} \|u_{\mu} \circ \Psi_{\mathbf{a}}^{\text{hf}} - u_{\bar{\mu}}\|_2^2 dX, \quad (15a)$$

where $u_{\mu}, u_{\bar{\mu}}$ are pre-processed to enforce that $\inf u_{\mu} = \inf u_{\bar{\mu}}$ and $\sup u_{\mu} = \sup u_{\bar{\mu}}$. If $\mathfrak{f}(\mathbf{a}_{\text{hf}}^k, \mu^k, \bar{\mu}) = 0$ for $k = 1, \dots, n_{\text{train}}$, we have that the whole snapshot set reduces to a point in \mathcal{U} in the mapped configuration. We also remark that $\mathfrak{f}(\mathbf{0}, \bar{\mu}, \bar{\mu}) = 0$: this implies that the identity map is a solution to (14) for $\mu = \bar{\mu}$.

For piecewise-constant functions, the choice (15a) is inappropriate due to the difficulties in computing $\nabla_{\mathbf{a}} \mathfrak{f}$. This is the case of geometry reduction³ in which the natural choice of u is the indicator function associated with Ω_{μ} , $u_{\mu} = \mathbb{1}_{\Omega_{\mu}}$. We denote by Γ_{μ} the discontinuity set of u_{μ} and by $\bar{\Gamma} = \Gamma_{\bar{\mu}}$ the discontinuity set of $\bar{u} = u_{\bar{\mu}}$; then, we introduce the *control points* $\{\mathbf{X}_i\}_{i=1}^{N_{\text{bnd}}} \subset \bar{\Gamma}$ and the corresponding "displaced" control points $\{\mathbf{x}_i^{\mu}\}_{i=1}^{N_{\text{bnd}}} \subset \Gamma_{\mu}$. Finally, we introduce the proximity measure

$$\mathfrak{f}(\mathbf{a}, \mu, \bar{\mu}) := \sum_{i=1}^{N_{\text{bnd}}} \|\Psi_{\mathbf{a}}^{\text{hf}}(\mathbf{X}_i) - \mathbf{x}_i^{\mu}\|_2^2. \quad (15b)$$

As discussed in section 4, construction of the dataset of pairs $\{(\mathbf{X}_i, \mathbf{x}_i^{\mu})\}_i$ in (15b) involves either the definition of a parameterization of the boundary $\partial\Omega_{\mu}$ or an explicit description of the deformation map $\mathbf{d}_{\mu} : \mathbf{X} \in \bar{\Gamma} \mapsto \mathbf{x}^{\mu} \in \Gamma_{\mu}$. Next Remark provides an alternative that does not require the definition of \mathbf{d}_{μ} , for a specific class of surfaces.

Remark 2.1. *Implicit surfaces.* If Γ_{μ} is represented implicitly as $\Gamma_{\mu} = \{\mathbf{x} \in \mathbb{R}^d : G_{\mu}(\mathbf{x}) = 0\}$ for $G_{\mu} : \mathbb{R}^d \rightarrow \mathbb{R}$, then we might consider the proximity measure:

$$\mathfrak{f}(\mathbf{a}, \mu, \bar{\mu}) = \sum_{i=1}^{N_{\text{bnd}}} |G_{\mu}(\Psi_{\mathbf{a}}^{\text{hf}}(\mathbf{X}_i))|^2$$

where $\{\mathbf{X}_i\}_i$ is a set of control points on $\bar{\Gamma}$. We do not consider this choice in the numerical experiments.

³ In geometry reduction, it is convenient to set $\bar{u} = \mathbb{1}_{\Omega}$ and then apply the registration method discussed here to $u_{\mu}, \bar{u} \in L^2(\Omega_{\text{box}})$, where Ω_{box} is a domain containing Ω, Ω_{μ} for all $\mu \in \mathcal{P}$. We refer to section 4 for further details.

2.2.2 Implementation

We resort to the Matlab routine `fmincon` [32] to solve (14): the routine relies on an interior point method ([9]) to find local minima of (14). In our implementation, we first reorder the snapshots such that

$$\mu^{(k+1)} := \arg \min_{\mu \in \Xi_{\text{train}} \setminus \{\mu^{(i)}\}_{i=1}^k} \|\mu^{(k)} - \mu\|_2, \quad \mu^{(1)} = \mu^1, \quad \Xi_{\text{train}} = \{\mu^k\}_{k=1}^{n_{\text{train}}}, \quad (16a)$$

and then we choose the initial conditions $\mathbf{a}_0^{(k)}$ for the k -th optimization problem as

$$\mathbf{a}_0^{(1)} = \mathbf{0}, \quad \mathbf{a}_0^{(k)} = \mathbf{a}_{\text{hf}}^{(k-1)}, \quad k = 2, \dots, n_{\text{train}}. \quad (16b)$$

Since the problem is non-convex and thus the solution is not guaranteed to be unique and to depend continuously on μ , we envision that $\mathbf{a}_{\text{hf}}^{(k)}$ might be far from $\mathbf{a}_{\text{hf}}^{(k-1)}$ even if $\|\mu^{(k)} - \mu^{(k-1)}\|_2$ is small: this makes the generalization step (cf. section 2.3) extremely challenging. For this reason, we propose to add the box constraints:

$$-C_\infty \|\mu^{(k)} - \mu^{(k-1)}\|_2 \leq (\mathbf{a}_{\text{hf}})_m - \left(\mathbf{a}_{\text{hf}}^{(k-1)}\right)_m \leq C_\infty \|\mu^{(k)} - \mu^{(k-1)}\|_2, \quad (16c)$$

for $m = 1, \dots, M$. In all our experiments, we set $C_\infty = 10$: for this choice of C_∞ , we have empirically found that this set of box constraints is not active at the local minima, for none of the cases considered.

In our numerical experiments, `fmincon` converges to local minima in $10^2 - 10^3$ iterations; the computational cost on a commodity laptop is $\mathcal{O}(1 - 5[\text{s}])$ for all tests run. We emphasize that for the examples of sections 3.3.1 and 3.3.2 the use of a structured grid, which allows rapid evaluations of $u^k \circ \Psi_{\mathbf{a}}^{\text{hf}}$ in the quadrature points is key to reduce computational costs.

2.2.3 Connection with optimal transport

Let us assume that u, \bar{u} are probability measures over Ω , that is $u, \bar{u} \geq 0$ and $\int_{\Omega} u \, dx = \int_{\Omega} \bar{u} \, dx = 1$. Then, Φ^{opt} is an optimal transport map if it is a global minimizer of

$$\min_{\Phi: \Omega \rightarrow \Omega} \int_{\Omega} \|\mathbf{X} - \Phi(\mathbf{X})\|_2^2 \, dX \quad \text{s.t. } \bar{u}(\mathbf{X}) = u(\Phi(\mathbf{X})) \mathfrak{J}(\mathbf{X}) \quad \forall \mathbf{X} \in \Omega, \quad (17)$$

where $\mathfrak{J} = \det(\hat{\nabla} \Phi)$. A barrier method to solve (17) reads as

$$\min_{\Phi: \Omega \rightarrow \Omega} \int_{\Omega} (\bar{u}(\mathbf{X}) - u(\Phi(\mathbf{X})) \mathfrak{J}(\mathbf{X}))^2 \, dX + \frac{1}{\lambda} \int_{\Omega} \|\mathbf{X} - \Phi(\mathbf{X})\|_2^2 \, dX, \quad (18)$$

where $\lambda \gg 1$.

The first addend in (18) is closely linked to the proximity measure \mathfrak{f} in (15a), while the second term can be interpreted as a measure of the deviation of Φ from the identity map, exactly as $|\Phi|_{H^2(\Omega)}$. Note, however, that there are important differences between (14) and (18). First, in (18), the functions u, \bar{u} should be probability measures, while in (14) u, \bar{u} are arbitrary real-valued functions in a Hilbert spaces \mathcal{U} contained in $L^2(\Omega)$. Second, if $u, \bar{u} \geq 0$, solutions to (14) do not in general conserve mass. Third, if u, \bar{u} are compactly supported in Ω , solutions to (17) are not guaranteed to be locally invertible in Ω .

2.3 Generalization

Given the dataset of pairs $\{\mu^k, \mathbf{a}_{\text{hf}}^k\}_{k=1}^{n_{\text{train}}}$, we resort to a multi-variate multi-target regression procedure to compute the mapping Φ_μ of the form (8) (cf. Algorithm 1 Line 4). First, we resort to POD (based on the Euclidean inner product) to determine a low-dimensional approximation of $\{\mathbf{a}_{\text{hf}}^k\}_k$:

$$\mathbf{a}_{\text{hf}}^k \approx \mathbf{U}_\Phi \mathbf{a}^k, \quad \mathbf{U}_\Phi \in \mathbb{R}^{M_{\text{hf}}, M}, \quad \mathbf{U}_\Phi^T \mathbf{U}_\Phi = \mathbb{1}_M, \quad M < M_{\text{hf}}. \quad (19a)$$

Then, we build the regressors $\hat{a}_m : \mathcal{P} \rightarrow \mathbb{R}$ based on the datasets $\{(\mu^k, a_{\text{hf}}^{m,k})\}_{k=1}^{n_{\text{train}}}$, $a_{\text{hf}}^{m,k} := (\mathbf{U}_\Phi^T \mathbf{a}_{\text{hf}}^k)_m$, for $m = 1, \dots, M$; finally, we return the mapping

$$\Phi_\mu(\mathbf{X}) = \mathbf{X} + \sum_{m=1}^M (\hat{\mathbf{a}}_\mu)_m \varphi_m(\mathbf{X}), \quad \begin{cases} \hat{\mathbf{a}} := [\hat{a}_1, \dots, \hat{a}_M]^T \\ \varphi_m(\mathbf{X}) = \sum_{m'=1}^{M_{\text{hf}}} (\mathbf{U}_\Phi)_{m',m} \varphi_{m'}^{\text{hf}}(\mathbf{X}) \end{cases} \quad (19b)$$

Some comments are in order. First, application of POD in (19a) leads to a (potentially substantial) reduction of the size of the mapping expansion and thus ultimately to a reduction of online costs; application of POD also reduces the importance of the choice of M_{hf} in (11) since it provides an automatic way of choosing the size of the expansion at the end of the offline stage. Note that, since POD is linear, the resulting expansion satisfies boundary conditions in (11b): applying Lemma 2.1, we find that the set

$$A_{\varphi, \epsilon} := \left\{ \mathbf{a} \in \mathbb{R}^M : \Phi = \mathbf{X} + \sum_m a_m \varphi_m(\mathbf{X}) \text{ satisfies (5)} \right\} \quad (20)$$

contains balls of finite radius centered in $\mathbf{0}$ for any $\epsilon > 0$. Second, any linear or nonlinear strategy for multivariate regression can be employed to construct $\hat{\mathbf{a}}$ based on $\{\mu^k, \mathbf{a}_{\text{hf}}^k\}_{k=1}^{n_{\text{train}}}$: in this work, we resort to a kernel-based Ridge regression procedure based on inverse multiquadric RBFs ([59]). Third, we remark that the mapping Φ_μ is not guaranteed to be bijective for all $\mu \in \mathcal{P}$, particularly for small-to-moderate values of n_{train} : this represents a major issue of the methodology that will be addressed in a subsequent work. We remark, nevertheless, that our approach is able to provide accurate and stable results for $n_{\text{train}} = \mathcal{O}(10^2)$ for all test cases considered in this paper. Finally, given the eigenvalues $\{\lambda_i\}_{i=1}^{n_{\text{train}}}$ of the POD Kernel matrix $\mathbf{C}_{k,k'} := \mathbf{a}^k \cdot \mathbf{a}^{k'}$, we choose M in (19a) such that

$$M := \min \left\{ M' : \sum_{m=1}^{M'} \lambda_m \geq (1 - \text{tol}_{\text{POD}}) \sum_{i=1}^{n_{\text{train}}} \lambda_i \right\}, \quad (21)$$

for some problem-dependent tolerance $\text{tol}_{\text{POD}} > 0$ that will be specified in the numerical sections.

3 Data compression

We discuss here how to exploit the procedure introduced in section 2 to tackle problem (1).

3.1 Computational procedure

Given (1), we compute problem-dependent mappings based on either the solution z_μ itself or selected coefficients of the PDE; then we apply pMOR (Reduced Basis) linear techniques to the resulting mapped problem (3). Algorithm 2 summarizes the (abstract) computational procedure. We conclude this section with three remarks.

Algorithm 2 pMOR with Lagrangian nonlinear data compression. Offline/online decomposition.

Offline stage

- 1: Build the dataset $\{\mu^k, u^k = u_{\mu^k}\}_{k=1}^{n_{\text{train}}}$.
- 2: Compute the mapping $\{\Phi_\mu : \mu \in \mathcal{P}\}$ based on $\{\mu^k, u^k\}_{k=1}^{n_{\text{train}}}$ (cf. section 2).
- 3: Generate the ROM for (3).

Online stage

- 1: Given $\bar{\mu}$, query the ROM to estimate $\hat{\mathbf{y}}_{\bar{\mu}}$ and the error $\|\hat{\mathbf{y}}_{\bar{\mu}} - \mathbf{y}_{\bar{\mu}}\|_2$.

Remark 3.1. Online mapping construction. In the proposed approach, the mapping Φ_μ is built during the offline stage. The construction relies on a regression algorithm to determine a parametric function $\hat{\mathbf{a}} : \mathcal{P} \rightarrow \mathbb{R}^M$. Following [34], we might resort to a projection-based (Galerkin, Petrov-Galerkin,...) formulation to simultaneously build the (reduced) mapping coefficients $\hat{\mathbf{a}}_\mu \in \mathbb{R}^M$ and the solution coefficients $\hat{\mathbf{a}}_\mu$ during the online stage, for any new value of the parameter μ . Note that the problem of simultaneously estimating $\hat{\mathbf{a}}_\mu$ and $\hat{\mathbf{a}}_\mu$ is highly nonlinear and non-convex even for linear problems: the offline construction of the map simplifies the implementation of the online projection step and ultimately reduces online costs, at the price of a more expensive offline stage. We refer to a future work for a thorough comparison of the two approaches.

Remark 3.2. Error estimation. As discussed in the introduction, in pMOR it is key to estimate the prediction error. For second-order elliptic problems, if we consider the norm⁴ $\|\cdot\| := \sqrt{\int_\Omega \|\nabla \cdot\|_2^2 dx}$, it is straightforward to verify that

$$\mathfrak{c}_\mu \|\tilde{z}_\mu - \hat{z}_\mu\| \leq \|z_\mu - \hat{z}_\mu \circ \Phi_\mu^{-1}\| \leq \mathfrak{C}_\mu \|\tilde{z}_\mu - \hat{z}_\mu\|,$$

where \hat{z}_μ denotes a generic approximate solution to (3), $\mathfrak{c}_\mu = \min_{\mathbf{X} \in \bar{\Omega}} \lambda_{\min}(\mathbf{K}_\mu)$, $\mathfrak{C}_\mu = \max_{\mathbf{X} \in \bar{\Omega}} \lambda_{\max}(\mathbf{K}_\mu)$, and $\mathbf{K}_\mu = \mathfrak{J}_\mu \hat{\nabla} \Phi_\mu^{-1} \hat{\nabla} \Phi_\mu^{-T}$. Provided that $\mathfrak{c}_\mu, \mathfrak{C}_\mu = \mathcal{O}(1)$, traditional residual-based error estimates (see, e.g., [46, Chapter 3]) in the mapped configuration can be used to sharply bound the prediction error $\|z_\mu - \hat{z}_\mu \circ \Phi_\mu^{-1}\|$.

Remark 3.3. Pointwise estimation of z_μ . Computation of $\hat{z}_\mu \circ \Phi_\mu^{-1}(\mathbf{x})$ for a given $\mathbf{x} \in \Omega$ involves the evaluation of $\Phi_\mu^{-1}(\mathbf{x})$, which requires the solution to the nonlinear problem

$$\min_{\mathbf{X} \in \bar{\Omega}} \|\Phi_\mu(\mathbf{X}) - \mathbf{x}\|_2.$$

In this work, we do not address the issue of how to efficiently evaluate $\hat{z}_\mu \circ \Phi_\mu^{-1}$.

⁴Similar estimates can be obtained for other norms.

3.2 Two-level approximations and N - M Kolmogorov widths

We can interpret Lagrangian approximations as two-level approximations of parametric fields, $z_\mu(\mathbf{x}) \approx \hat{z}_\mu(\Phi_\mu^{-1}(\mathbf{x}))$: the inner layer corresponds to the mapping process, while the outer layer is associated with the linear approximation. This observation highlights the connection between Lagrangian approaches and deep networks. We can also generalize the Kolmogorov N -width (4) to Lagrangian approximations. Given the integers $N, M > 0$ and the tolerance $\epsilon \in (0, 1)$, we define (see also [49])

$$d_{N,M,\epsilon}(\mathcal{M}) := \inf_{(\{\varphi_m\}_m, \mathbf{a})} d_N \left(\widetilde{\mathcal{M}}(\{\varphi_m\}_m, \mathbf{a}) \right), \quad (22)$$

where $\widetilde{\mathcal{M}}(\{\varphi_m\}_m, \mathbf{a}) := \{z_\mu \circ \Phi_\mu : \mu \in \mathcal{P}\}$ with $\Phi_\mu = \mathbf{X} + \sum_m (\mathbf{a}_\mu)_m \varphi_m(\mathbf{X})$, and the infimum is taken over all pairs $(\{\varphi_m\}_m, \mathbf{a}) \in [\text{Lip}(\Omega; \mathbb{R}^d)]^M \times C(\mathcal{P}, A_{\varphi, \epsilon})$ and $A_{\varphi, \epsilon}$ is defined in (20). Note that, for any $N, M \geq 1$, $d_{N,M,\epsilon}(\mathcal{M}) \leq d_N(\mathcal{M})$, $d_{N,0,\epsilon}(\mathcal{M}) = d_N(\mathcal{M})$, and $d_{N,M,\epsilon=1}(\mathcal{M}) = d_N(\mathcal{M})$.

As for deep vs shallow networks ([45]), the use of Lagrangian methods for a given class of problems for pMOR should be supported by evidence of their superior approximation power compared to linear approaches. Next two examples provide insights about two classes of parametric problems for which Lagrangian methods might be effective.

Example 3.1. Boundary layers. We consider the one-dimensional problem:

$$\begin{cases} -\partial_{xx} z_\mu + \mu^2 z_\mu = 0 & \text{in } \Omega_{1D} = (0, 1) \\ z_\mu(0) = 1, \quad \partial_x z_\mu(1) = 0, \end{cases} \quad (23)$$

where $\mu \in \mathcal{P} := [\mu_{\min}, \mu_{\max} = \epsilon^{-2} \mu_{\min}]$. Provided that $\mu_{\min} \gg 1$, the solution to (23) can be approximated as $z_\mu(x) \approx e^{-\mu x}$ for all $\mu \in \mathcal{P}$ and $x \in \Omega_{1D}$. We introduce the parametrically-affine ($M = 1$) mapping

$$\Phi_\mu(X) = X + c_\mu \left(X \mathbb{1}_{[0,\delta)}(X) + \frac{\delta}{\delta - 1} (X - 1) \mathbb{1}_{[\delta,1]}(X) \right), \quad c_\mu := \frac{\bar{\mu} - \mu}{\mu},$$

which is a bijection in $[0, 1]$ for $0 < \delta < \min \left\{ 1, \frac{\mu}{\bar{\mu}} \right\}$, and we set

$$\bar{\mu} = \sqrt{\mu_{\min} \mu_{\max}}, \quad \delta = \frac{\epsilon}{1 + \epsilon}. \quad (24)$$

Note that for this choice⁵ of $\bar{\mu}$ and δ we find that Φ_μ satisfies (5) for all $\mu \in \mathcal{P}$. In conclusion, we find

$$\|z_{\bar{\mu}} - z_\mu \circ \Phi_\mu\|_{L^2(\Omega)} \approx \sqrt{\int_\delta^1 (e^{-\bar{\mu}X} - e^{-\mu \Phi_\mu(X)})^2 dX} \leq \sqrt{1 - \delta} e^{-\bar{\mu}\delta},$$

which implies that

$$d_{N=1, M=1, \epsilon}(\mathcal{M}) \lesssim \sqrt{1 - \delta} e^{-\bar{\mu}\delta}.$$

The latter is small for $\bar{\mu}\delta = \frac{\mu_{\min}}{1 + \epsilon} \gg 1$.

⁵ In particular, the choice of $\bar{\mu}$ in (24) minimizes the maximum value attained by either the Jacobian of the mapping or by the Jacobian of the inverse Φ_μ^{-1} over \mathcal{P} in $X = 0$, $\max_{\mu \in \mathcal{P}} \max \left\{ \partial_X \Phi_\mu(0), \partial_x \Phi_\mu^{-1}(0) \right\}$.

Example 3.2. Shock waves. We consider the manifold ([38, section 5.1], [54, Example 2.5])

$$\mathcal{M} := \{z(\cdot; t) = \text{sign}(\cdot - t - 1/3) : t \in [0, 1/3]\} \subset L^2(\Omega_{1D} = (0, 1)),$$

which is associated with the transport problem

$$\begin{cases} \partial_t z + \partial_x z = 0 & x \in \Omega_{1D}, t \in (0, 1/3), \\ z(x)|_{t=0} = \text{sign}(x - \frac{1}{3}), \quad z(0, t) = -1 & x \in \Omega_{1D}, t \in (0, 1/3), \end{cases}$$

with time interpreted as parameter. It is possible to show (see [38, section 5.1]) that the Kolmogorov N -width associated with \mathcal{M} satisfies $d_N(\mathcal{M}) = \mathcal{O}\left(\frac{1}{\sqrt{N}}\right)$. On the other hand, if we consider the parametrically-affine ($M = 1$) mapping

$$\Phi(X; t) := X + \left(2t - \frac{1}{3}\right) (X \mathbb{1}_{[0, 1/2]}(X) + (1 - X) \mathbb{1}_{[1/2, 1]}(X)), \quad (25)$$

we find $\tilde{z}(X, t) = \text{sign}(2X - 1)$, which is parameter-independent. This implies that

$$d_{N, M, \epsilon}(\mathcal{M}) = 0, \quad \forall N, M \geq 1, \quad \epsilon \leq \frac{2}{3}.$$

This example suggests that mapping procedures are well-suited to tackle problems with travelling fronts. On the other hand, we observe that Φ in (25) is not well-defined for $t \geq \frac{2}{3}$: the reason is that the shock/jump discontinuity exits the domain. This shows that effective applications of our approach to general parametric problems might require the partition of the time/parameter domain in several subdomains.

3.3 Numerical results

3.3.1 Approximation of boundary layers

Problem statement

We consider the diffusion-reaction problem:

$$\begin{cases} -\Delta z_\mu + \mu^2 z_\mu = 0 & \text{in } \Omega = (0, 1)^2 \\ z_\mu = 1 & \text{on } \Gamma_D := \{\mathbf{x} \in \partial\Omega : x_1 = 0 \text{ or } x_2 = 0\}, \\ \partial_n z_\mu = 0 & \text{on } \Gamma_N := \partial\Omega \setminus \Gamma_D, \end{cases} \quad (26)$$

where $\mu \in \mathcal{P} = [\mu_{\min}, \mu_{\max}]$, $\mu_{\min} = 20, \mu_{\max} = 200$. For large values of μ , the solution exhibits a boundary layer at Γ_D . By exploiting a standard argument, we can derive the variational formulation for the lifted field $\dot{z}_\mu := z_\mu - 1 \in \mathcal{X} := H_{0, \Gamma_D}^1(\Omega)$:

$$\mathcal{G}_\mu(\dot{z}_\mu, v) := \int_{\Omega} \nabla \dot{z}_\mu \cdot \nabla v \, dx + \mu^2 \int_{\Omega} (\dot{z}_\mu + 1) v \, dx = 0 \quad \forall v \in \mathcal{X}. \quad (27)$$

Given the parametric mapping $\Phi_\mu : \Omega \rightarrow \Omega$ such that $\Phi_\mu(\Gamma_D) = \Gamma_D$, we find that $\tilde{z}_\mu = \dot{z}_\mu \circ \Phi_\mu \in \mathcal{X}$ satisfies:

$$\mathcal{G}_{\mu, \Phi}(\tilde{z}_\mu, v) := \int_{\Omega} \mathbf{K}_\mu \hat{\nabla} \tilde{z}_\mu \cdot \hat{\nabla} v \, dX + \mu^2 \int_{\Omega} \mathfrak{J}_\mu (\tilde{z}_\mu + 1) v \, dX = 0 \quad \forall v \in \mathcal{X}, \quad (28)$$

where $\mathbf{K}_\mu = \mathfrak{J}_\mu \widehat{\nabla} \Phi_\mu^{-1} \widehat{\nabla} \Phi_\mu^{-T}$ and $\mathfrak{J}_\mu = \det(\widehat{\nabla} \Phi_\mu)$. We here resort to a continuous P3 FE discretization with $N_{\text{hf}} = 11236$ degrees of freedom on a structured triangular mesh. The grid is refined close to the boundary Γ_D , to accurately capture the boundary layer.

Construction of the mapping

We here propose to employ Algorithm 1 to obtain the empirical mapping Φ_μ to be used in (28). Towards this end, recalling the discussion in Example 3.1, we set $\bar{\mu} = \sqrt{\mu_{\min} \mu_{\max}}$. We further consider the proximity measure \mathfrak{f} in (15a) with $u_\mu = z_\mu$, we set $\epsilon = 0.1$, $\xi = 10^{-10}$, and we consider a polynomial expansion with $M = 8$ in (13) ($M_{\text{hf}} = 128$). To build the regressor $\widehat{\mathbf{a}} : \mathcal{P} \rightarrow \mathbb{R}^M$, we consider $n_{\text{train}} = 70$ log-equispaced parameters in \mathcal{P} , and we set $\text{tol}_{\text{pod}} = 10^{-4}$ in (21): for this choice of the parameters, Algorithm 1 returns an affine expansion with $M = 5$ terms.

Results

Figure 2(a) shows the behavior of the solution field z_μ for $\mu = 20$; as anticipated above, the solution exhibits a boundary layer close to Γ_D . In Figure 2(b) and (c), we show slices of the solution field for three parameter values along the straight lines depicted in Figure 2(a): as expected, the size of the boundary layer strongly depends on the value of μ . In Figure 3, we reproduce the results of Figure 2 for the mapped field: we observe that the mapping procedure significantly reduces the sensitivity of the solution to the value of μ .

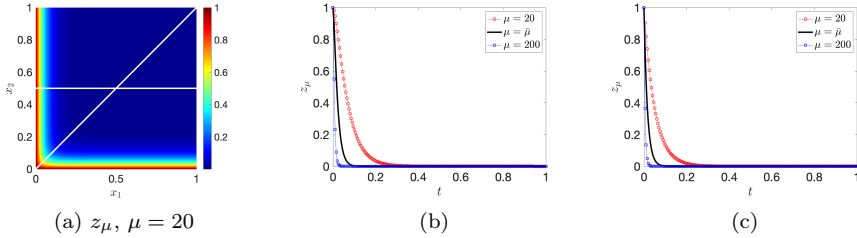


Figure 2: reaction-diffusion problem with boundary layer. (a): behavior of $z_{\mu=20}$. (b) and (c): behavior of $z_\mu(\mathbf{x} = (t, t))$ and $z_\mu(\mathbf{x} = (t, 0.5))$ for three values of $\mu \in \mathcal{P}$, $t \in [0, 1]$.

Figure 4 shows the behavior of the relative H^1 projection error associated with the POD space in the physical (unregistered) and mapped (registered) configurations,

$$E_{\text{proj}} = \max_{\mu \in \{\mu^j\}_{j=1}^{n_{\text{test}}} \sim \text{Uniform}(\mathcal{P})} \frac{\|z_\mu - \Pi_{\mathcal{Z}_N} z_\mu\|_{H^1(\Omega)}}{\|z_\mu\|_{H^1(\Omega)}}, \quad \tilde{E}_{\text{proj}} = \max_{\mu \in \{\mu^i\}_{i=1}^{n_{\text{test}}} \sim \text{Uniform}(\mathcal{P})} \frac{\|\tilde{z}_\mu - \Pi_{\tilde{\mathcal{Z}}_N} \tilde{z}_\mu\|_{H^1(\Omega)}}{\|\tilde{z}_\mu\|_{H^1(\Omega)}}, \quad (29)$$

where $\mu^1, \dots, \mu^{n_{\text{test}}} \stackrel{\text{iid}}{\sim} \text{Uniform}(\mathcal{P})$ ($n_{\text{test}} = 200$) and the spaces $\{\mathcal{Z}_N\}_N$ and $\{\tilde{\mathcal{Z}}_N\}_N$ are built using POD based on the $H^1(\Omega)$ inner product and on the snapshot sets $\{z_{\mu^i}\}_{i=1}^{n_{\text{test}}}$ and $\{\tilde{z}_{\mu^i}\}_{i=1}^{n_{\text{test}}}$, respectively. Note that $\tilde{E}_{\text{proj}} \leq E_{\text{proj}}$

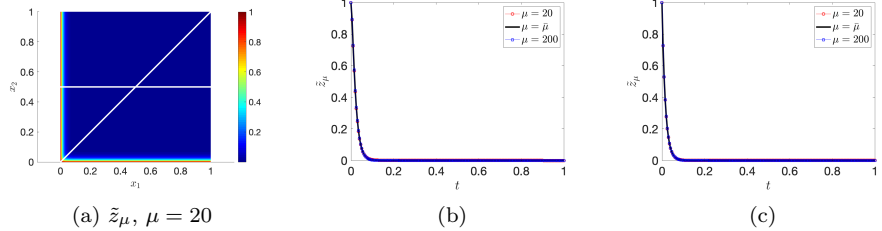


Figure 3: reaction-diffusion problem with boundary layer. (a): behavior of $\tilde{z}_{\mu=20}$. (b) and (c): behavior of $\tilde{z}_\mu(\mathbf{X} = (t, t))$ and $\tilde{z}_\mu(\mathbf{X} = (t, 0.5))$ for three values of $\mu \in \mathcal{P}$, $t \in [0, 1]$.

for $N \leq 6$, while $\tilde{E}_{\text{proj}} > E_{\text{proj}}$ for $N > 6$; to investigate the relation between \tilde{E}_{proj} and E_{proj} , in Figure 4(b) we show the $H^1(\Omega)$ -POD eigenvalues associated with $\{z_{\mu^i}\}_{i=1}^{n_{\text{test}}}$ (unregistered) and $\{\tilde{z}_{\mu^i}\}_{i=1}^{n_{\text{test}}}$ (registered), while in Figure 4(c) we show the $L^2(\Omega)$ -POD eigenvalues associated with $\{\mathbf{K}_{\mu^i}\}_{i=1}^{n_{\text{test}}}$. The decay rate of the eigenvalues associated with $\{\mathbf{K}_{\mu^i}\}_{i=1}^{n_{\text{test}}}$ is much slower than the decay rate of the eigenvalues associated with $\{z_{\mu^i}\}_{i=1}^{n_{\text{test}}}$: we envision that the "complexity overhead" associated with the mapping process might be responsible for the deterioration of the convergence rate for large values of N . Nevertheless, we do emphasize that for $N = 1$ the relative error satisfies $\tilde{E}_{\text{proj}} \lesssim 10^{-4}$ and is thus comparable with the accuracy of the underlying truth discretization. We remark that the decay of the POD eigenvalues cannot be directly related to the behavior of the Kolmogorov N -width; nevertheless, POD eigenvalues provides an heuristic measure of the linear complexity of parametric manifolds and are thus shown in this paper to investigate performance of the registration algorithm.

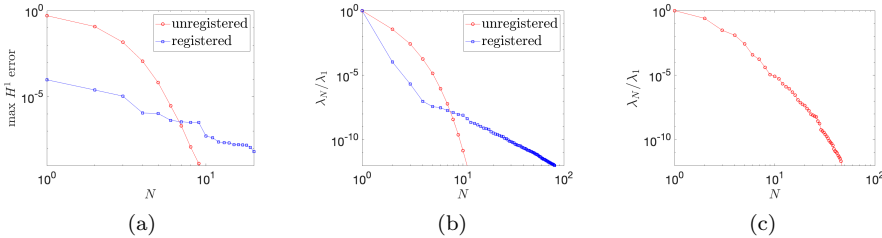


Figure 4: reaction-diffusion problem with boundary layer. (a): behavior of $E_{\text{proj}}, \tilde{E}_{\text{proj}}$ (29) with N . (b): behavior of the H^1 -POD eigenvalues associated with $\{z_{\mu^i}\}_{i=1}^{n_{\text{test}}}$ (unregistered) and $\{\tilde{z}_{\mu^i}\}_{i=1}^{n_{\text{test}}}$ (registered). (c): behavior of the L^2 -POD eigenvalues associated with $\{\mathbf{K}_{\mu^i}\}_{i=1}^{n_{\text{test}}}$.

3.3.2 Approximation of advection-dominated problems

Problem statement

We consider the advection-reaction problem:

$$\begin{cases} \nabla \cdot (\mathbf{c}_\mu z_\mu) + \sigma_\mu z_\mu = f_\mu & \text{in } \Omega = (0, 1)^2 \\ z_\mu = z_{D,\mu} & \text{on } \Gamma_{in,\mu} := \{\mathbf{x} \in \partial\Omega : \mathbf{c}_\mu \cdot \mathbf{n} < 0\} \end{cases} \quad (30a)$$

where \mathbf{n} denotes the outward normal to $\partial\Omega$, and

$$\begin{aligned} \mathbf{c}_\mu &= \begin{bmatrix} \cos(\mu_1) \\ \sin(\mu_1) \end{bmatrix}, \quad \sigma_\mu = 1 + \mu_2 e^{x_1+x_2}, \quad f_\mu = 1 + x_1 x_2, \\ z_{D,\mu} &= 4 \arctan \left(\mu_3 \left(x_2 - \frac{1}{2} \right) \right) (x_2 - x_2^2) \\ \mu &= [\mu_1, \mu_2, \mu_3] \in \mathcal{P} := \left[-\frac{\pi}{10}, \frac{\pi}{10} \right] \times [0.3, 0.7] \times [60, 100]. \end{aligned} \quad (30b)$$

Problem (30) is a parametric hyperbolic advection-reaction problem; since $\sigma_\mu + \frac{1}{2} \nabla \cdot \mathbf{c}_\mu \geq 1 > 0$ for all $\mathbf{x} \in \Omega, \mu \in \mathcal{P}$, there exists a unique solution z_μ to (30) for all $\mu \in \mathcal{P}$. Changes in μ_1 lead to changes in the large-gradient region associated with the solution z_μ (cf. Figures (5)(a) and (b)), and are thus critical for linear approximation methods. We refer to [8, 15] for a mathematical analysis of the problem, and for the derivation of the infinite-dimensional variational form. We further observe that, for any Lipschitz map Φ_μ , the mapped field $\tilde{z}_\mu = z_\mu \circ \Phi_\mu$ solves a problem of the form (30) with coefficients

$$\tilde{\mathbf{c}}_\mu := \mathfrak{J}_\mu \hat{\nabla} \Phi_\mu^{-1} \mathbf{c}_\mu \circ \Phi_\mu, \quad \tilde{\sigma}_\mu := \mathfrak{J}_\mu \sigma_\mu \circ \Phi_\mu, \quad \tilde{f}_\mu := \mathfrak{J}_\mu f_\mu \circ \Phi_\mu, \quad \tilde{z}_{D,\mu} := z_{D,\mu} \circ \Phi_\mu. \quad (31)$$

We here resort to a Discontinuous Galerkin (DG) P3 discretization on a structured triangular mesh with $N_{hf} = 23120$ degrees of freedom to approximate (30). Let \mathcal{X} be the broken DG space associated with the mesh $\{\mathbb{D}^k\}_{k=1}^{n_{el}}$, the DG discretization of (30) reads as follows: find $z_\mu \in \mathcal{X}$ such that

$$\begin{aligned} \mathcal{G}_\mu(z_\mu, v) &= \sum_{k=1}^{n_{el}} \int_{\mathbb{D}^k} \boldsymbol{\Upsilon}_\mu^{\text{el}} \cdot A^{\text{el}}(z_\mu, v) - f_\mu v \, dx \\ &\quad + \int_{\partial\mathbb{D}^k} \boldsymbol{\Upsilon}_\mu^{\text{ed}} \cdot A^{\text{ed}}(z_\mu, v) - f_\mu^{\text{ed}} v \, dx = 0, \quad \forall v \in \mathcal{X}. \end{aligned} \quad (32)$$

The vector-valued functions $\boldsymbol{\Upsilon}_\mu^{\text{el}}$, and $\boldsymbol{\Upsilon}_\mu^{\text{ed}}, f_\mu^{\text{ed}}$ and the parameter-independent bilinear operators $A^{\text{el}}, A^{\text{ed}}$ are introduced, together with the DG discretization, in Appendix C. We endow \mathcal{X} with the discrete L^2 inner product $(w, v) := \sum_{k=1}^{n_{el}} \int_{\mathbb{D}^k} w v \, dx$, and the induced norm $\|\cdot\| = \sqrt{(\cdot, \cdot)}$.

POD-Galerkin reduced-order model

To devise an online-efficient ROM to approximate z_μ , we introduce the parametrically-affine approximations $\boldsymbol{\Upsilon}_\mu^{\text{el,eim}}, f_\mu^{\text{eim}}, \boldsymbol{\Upsilon}_\mu^{\text{ed,eim}}, f_\mu^{\text{ed,eim}}$ of $\boldsymbol{\Upsilon}_\mu^{\text{el}}, f_\mu, \boldsymbol{\Upsilon}_\mu^{\text{ed}}, f_\mu^{\text{ed}}$, obtained using the Empirical Interpolation Method (EIM, [4]) and one of its

extensions to vector-valued fields (cf. [53, Appendix B])

$$\begin{aligned}\boldsymbol{\Upsilon}_\mu^{\text{el,eim}}(\mathbf{x}) &:= \sum_{q=1}^{Q_{\text{a,el}}} \Theta_{\mu,q}^{\text{el,a}} \boldsymbol{\Upsilon}_q^{\text{el}}(\mathbf{x}), \quad \boldsymbol{\Upsilon}_\mu^{\text{ed,eim}}(\mathbf{x}) := \sum_{q=1}^{Q_{\text{a,ed}}} \Theta_{\mu,q}^{\text{ed,a}} \boldsymbol{\Upsilon}_q^{\text{ed}}(\mathbf{x}), \\ f_\mu^{\text{eim}}(\mathbf{x}) &:= \sum_{q=1}^{Q_{\text{f,el}}} \Theta_{\mu,q}^{\text{el,f}} f_q^{\text{el}}(\mathbf{x}), \quad f_\mu^{\text{ed,eim}}(\mathbf{x}) := \sum_{q=1}^{Q_{\text{f,ed}}} \Theta_{\mu,q}^{\text{ed,f}} f_q^{\text{ed}}(\mathbf{x}).\end{aligned}\tag{33}$$

We refer to Appendix D for further details concerning the implementation of EIM. Then we substitute these approximations in (32) to obtain a parametrically-affine surrogate of \mathcal{G}_μ :

$$\begin{aligned}\mathcal{G}_\mu^{\text{eim}}(z_\mu^{\text{eim}}, v) &= \sum_{k=1}^{n_{\text{el}}} \int_{\mathbb{D}^k} \boldsymbol{\Upsilon}_\mu^{\text{el,eim}} \cdot A^{\text{el}}(z_\mu^{\text{eim}}, v) - f_\mu^{\text{eim}} v \, dx \\ &\quad + \int_{\partial\mathbb{D}^k} \boldsymbol{\Upsilon}_\mu^{\text{ed,eim}} \cdot A^{\text{ed}}(z_\mu^{\text{eim}}, v) - f_\mu^{\text{ed,eim}} v \, dx = 0, \quad \forall v \in \mathcal{X}.\end{aligned}$$

Then, given the reduced space $\mathcal{Z}_N := \text{span}\{\zeta_n\}_{n=1}^N \subset \mathcal{X}$, we define the Galerkin ROM:

$$\text{find } \hat{z}_\mu \in \mathcal{Z}_N : \mathcal{G}_\mu^{\text{eim}}(\hat{z}_\mu, v) = 0 \quad \forall v \in \mathcal{Z}_N.\tag{34}$$

We resort to POD to build the reduced space \mathcal{Z}_N . We choose the size of the expansions in (33) using the criterion in (21): we here consider the tolerance $\text{tol}_{\text{eim}} = 5 \cdot 10^{-7}$.

We remark that the weak or strong Greedy algorithms could also be used to build the space \mathcal{Z}_N ; similarly, we might also rely on Petrov-Galerkin (minimum residual) projection to estimate the solution, and we might also consider several other hyper-reduction techniques to achieve online efficiency. Since the focus of this paper is to assess the performance of the mapping procedure, we do not further discuss these aspects in the remainder. Finally, we remark that in this section we discussed how to determine a Galerkin ROM in the physical configuration: since the mapped problem shares the same structure, the corresponding Galerkin ROM is also of the form (34).

Construction of the mapping

We set $\bar{\mu}$ equal to the centroid of \mathcal{P} , and we consider the proximity measure \mathfrak{f} in (15a) with $u_\mu = z_\mu$. We further consider $\epsilon = 0.1$, $\xi = 10^{-3}$, and we consider a polynomial expansion with $\bar{M} = 6$ in (13) ($M_{\text{hf}} = 72$). To build the regressor $\hat{\mathbf{a}} : \mathcal{P} \rightarrow \mathbb{R}^M$, we consider $n_{\text{train}} = 250$ uniformly-sampled parameters in \mathcal{P} , and we set $\text{tol}_{\text{pod}} = 10^{-4}$ in (21): for this choice of the parameters, Algorithm 1 returns an affine expansion with $M = 12$ terms.

As opposed to the previous problem, we do not expect that the mapping procedure will lead to a nearly one-dimensional mapped manifold; nevertheless, we do expect that the mapping procedure will reduce the sensitivity of the solution to parametric changes, particularly in μ_1 — which regulates the position of the high-gradient region in Ω . For this reason, we here consider a larger value of the regularization parameter ξ compared to the previous two examples: larger values of ξ lead to smoother mappings and thus reduce the risk of overfitting and facilitate hyper-reduction. We further consider a lower value of M_{hf} ($M_{\text{hf}} = 72$ as opposed to $M_{\text{hf}} = 128$) compared to the previous example: in our numerical experience, the algorithm is insensitive to the choice of M_{hf} , for $M_{\text{hf}} \geq 72$.

Results

Figure 5 shows the solution to (30) for three values of the parameters $\mu^1 = [-\pi/10, 0.3, 60]$, $\mu^2 = [\pi/10, 0.7, 100]$ and the centroid $\bar{\mu} = [0, 0.55, 80]$; on the other hand, Figure 6 shows the solution to the mapped problem $\tilde{z}_\mu = z_\mu \circ \Phi_\mu$ for the same three values of the parameter. As stated above, changes in μ_1 lead to changes in the large-gradient region which corresponds to the propagation of the inflow boundary condition in the interior of Ω : the mapping Φ_μ significantly reduces the sensitivity of the solution to changes in the angle μ_1 .

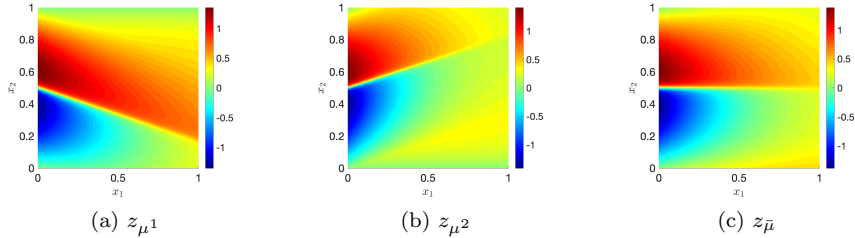


Figure 5: advection-reaction problem. Solution to (30) for three parameter values.

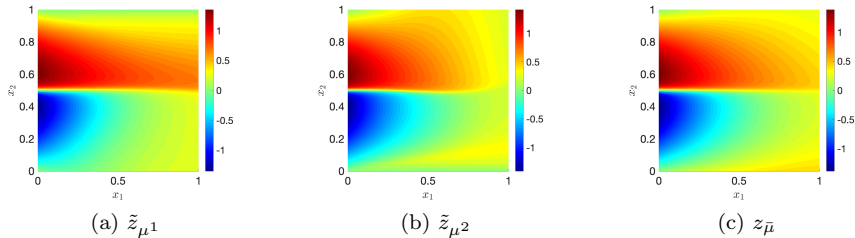


Figure 6: advection-reaction problem. Solution to (30) for three parameter values in the mapped configuration.

Figure 7(a) shows the behavior of the average relative L^2 error

$$E_{\text{avg}} := \frac{1}{n_{\text{test}}} \sum_{i=1}^{n_{\text{test}}} \frac{\|z_{\mu^i} - \tilde{z}_{\mu^i}\|_{L^2(\Omega)}}{\|z_{\mu^i}\|_{L^2(\Omega)}},$$

for the POD-Galerkin ROM associated with the unregistered configuration, and for the POD-Galerkin ROM associated with the registered configuration. Here, $\mu^1, \dots, \mu^{n_{\text{test}}} \stackrel{\text{iid}}{\sim} \text{Uniform}(\mathcal{P})$, $n_{\text{test}} = 20$. In order to use the same metric for both registered and unregistered ROMs, for the registered case we compute the error as

$$\|z_{\mu^i} - \tilde{z}_{\mu^i} \circ \Phi_\mu^{-1}\|_{L^2(\Omega)} = \sqrt{\int_{\Omega} \mathfrak{J}_\mu (\tilde{z}_{\mu^i} - \tilde{z}_{\mu^i})^2 dX}.$$

Figure 7(b) shows the $L^2(\Omega)$ -POD eigenvalues associated with $\{z_{\mu^i}\}_{i=1}^{n_{\text{train}}}$ (unregistered) and $\{\tilde{z}_{\mu^i}\}_{i=1}^{n_{\text{train}}}$ (registered).

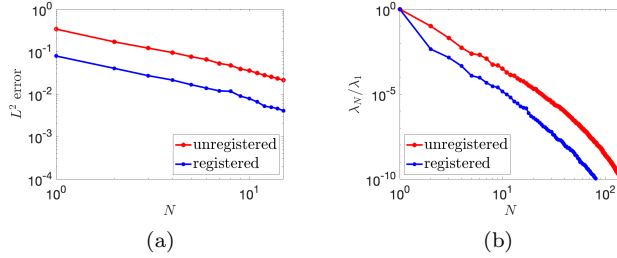


Figure 7: advection-reaction problem. (a): behavior of E_{avg} with N for the registered and unregistered POD-Galerkin ROMs. (b): behavior of $L^2(\Omega)$ -POD eigenvalues associated with $\{z_{\mu^i}\}_{i=1}^{n_{\text{train}}}$ (unregistered) and $\{\tilde{z}_{\mu^i}\}_{i=1}^{n_{\text{train}}}$ (registered).

We observe that the decay rates of E_{avg} and of the POD eigenvalues are nearly the same for both registered and unregistered configurations; however, the multiplicative constant is significantly different: $E_{\text{avg}}^{\text{reg.}} \approx \frac{1}{4} E_{\text{avg}}^{\text{unreg.}}$ for all values of N considered, while $\left(\frac{\lambda_N}{\lambda_1}\right)^{\text{reg.}} \approx \frac{1}{100} \left(\frac{\lambda_N}{\lambda_1}\right)^{\text{unreg.}}$ for $N \geq 2$. As a result, for any given N , the nonlinear mapping procedure leads to a significant improvement. On the other hand, we observe that for this test case the mapping procedure leads to a significant increase in the number of EIM modes in (33): for the registered case, we have

$$Q_{\text{a,el}} = 19, \quad Q_{\text{a,ed}} = 26, \quad Q_{\text{f,el}} = 15, \quad Q_{\text{f,ed}} = 6;$$

for the unregistered case⁶, we have

$$Q_{\text{a,el}} = 4, \quad Q_{\text{a,ed}} = 3, \quad Q_{\text{f,el}} = 1, \quad Q_{\text{f,ed}} = 2.$$

Therefore, for any given N , the registered ROM is more expensive in terms of memory than the unregistered ROM.

4 Geometry reduction

We address below the problem of geometry reduction for pMOR applications. In section 4.1, we introduce two model problems considered in the numerical experiments; in this section, we also introduce notation, relevant definitions, and two representative techniques proposed in [50] and [31] that will serve as benchmark to assess our proposal. Then, in section 4.2, we discuss how to employ our registration algorithm to the two problems of interest. Finally, in section 4.3, we present the numerical validation.

⁶ Note that most coefficients in (30) are parametrically affine in the unregistered configuration.

4.1 Model problems

4.1.1 Diffusion problem with discontinuous coefficients

Problem statement

We consider the diffusion problem

$$-\nabla \cdot (\kappa_\mu \nabla z_\mu) = 1 \text{ in } \Omega, \quad z_\mu|_{\partial\Omega} = 0, \quad (35a)$$

where $\Omega = (0, 1)^2$, $\mu = [\mu_1, \mu_2] \in \mathcal{P} = [-0.05, 0.05]^2$ and the conductivity coefficient is given by

$$\kappa_\mu(\mathbf{x}) := 0.1 + 0.9 \mathbb{1}_{\Omega_{\text{in},\mu}}(\mathbf{x}), \quad \Omega_{\text{in},\mu} := \{\mathbf{x} \in \Omega : \|\mathbf{x} - \bar{\mathbf{x}}_\mu\|_\infty \leq \frac{1}{4}\}, \quad (35b)$$

with $\bar{\mathbf{x}}_\mu := [1/2 + \mu_1, 1/2 + \mu_2]$. The problem is a variant of the thermal block problem, which has been extensively considered in the Reduced Basis literature (see, e.g., [50, section 6.1.1]). We here approximate the solution to (35) through a continuous Galerkin P3 Finite Element (FE) discretization with $N_{\text{hf}} = 21025$ degrees of freedom.

Since κ_μ is piecewise constant with parameter-dependent jump discontinuities, pMOR techniques are not well-suited to directly tackle (35). It is thus necessary to introduce a mapping $\Phi : \Omega \times \mathcal{P} \rightarrow \Omega$ such that $\kappa_\mu \circ \Phi_\mu : \Omega \rightarrow \mathbb{R}$ is parameter-independent. From the geometry reduction viewpoint, given $\Omega_{\text{in}} := \Omega_{\text{in},\mu=0}$, we seek Φ such that (i) $\Phi_\mu(\Omega) = \Omega$ and (ii) $\Phi_\mu(\Omega_{\text{in}}) = \Omega_{\text{in},\mu}$ for all $\mu \in \mathcal{P}$. In view of the discussion, we introduce the mapped problem for a generic map $\Phi_\mu : \Omega \rightarrow \Omega$: find $\tilde{z}_\mu = z_\mu \circ \Phi_\mu \in \mathcal{X} := H_0^1(\Omega)$ such that

$$\int_{\Omega} \mathbf{K}_\mu \hat{\nabla} \tilde{z}_\mu \cdot \hat{\nabla} v \, dX = \int_{\Omega} \mathfrak{J}_\mu v \, dX, \quad \forall v \in \mathcal{X}, \quad (36a)$$

with

$$\mathbf{K}_\mu := \mathfrak{J}_\mu (\kappa_\mu \circ \Phi_\mu) \left(\hat{\nabla} \Phi_\mu \right)^{-1} \left(\hat{\nabla} \Phi_\mu \right)^{-T}, \quad \mathfrak{J}_\mu := \det \left(\hat{\nabla} \Phi_\mu \right). \quad (36b)$$

Automatic piecewise-affine maps

Since the deformation of $\Omega_{\text{in},\mu}$ is rigid, we might explicitly build a piecewise linear map Φ . First, we identify a set of *control points* — the black dots in Figure 8(a) — and we use them to build a coarse partition of Ω — shown in Figure 8(a) as well. Then, we define a mapping $\Phi = \Phi^{\text{aff}}$ such that (i) $\Phi_\mu^{\text{aff}}(\Omega_{\text{in}}) = \Omega_{\text{in},\mu}$ for all $\mu \in \mathcal{P}$, and (ii) Φ_μ^{aff} is piecewise linear in \mathbf{X} in all elements of the partition. Then, we define the mapped problem (36) with $\Phi_\mu = \Phi_\mu^{\text{aff}}$.

Note that, for this choice of the mapping, \mathbf{K}_μ and \mathfrak{J}_μ in (36b) are piecewise-constant in each element of the partition: this implies that (36) is *parametrically-affine* — that is, \mathbf{K}_μ and \mathfrak{J}_μ are linear combinations of parameter-dependent coefficients and parameter-independent spatial fields. Therefore, the solution \tilde{z}_μ can be efficiently approximated using standard pMOR (e.g., Reduced Basis) techniques.

Given the user-defined control points, Rozza et al. have developed in [50] an automatic procedure to generate the partition of Ω and to determine an economic piecewise-constant approximation of the form in (36). The latter relies

on symbolic manipulation techniques to identify redundant terms in the affine expansions. Furthermore, for the approach to be effective, we should consider FE triangulations that are conforming to the coarse-grained partition in Figure 8(a). Finally, the choice of the control points, which is trivial in this case, might not be straightforward for more challenging problems. In conclusion, even if the approach works remarkably well in many situations, practical implementation of the procedure in [50] is rather involved and highly problem-dependent.

4.1.2 Laplace's equation in parameterized domains

Problem statement

Given the parameter domain $\mathcal{P} = [0.1, 0.4]^2 \times [0, \pi/4]$, we first introduce the parametric closed curve $t \in [0, 2\pi) \mapsto \gamma_{\text{in},\mu}(t) \in \mathbb{R}^2$ such that

$$\gamma_{\text{in},\mu}(t) = \begin{bmatrix} \cos(t) \left(1 + \mu_1 (\cos(t + \mu_3))^2 + 2 \cdot 10^{-3} ((2\pi - t) t)^2\right) \\ \sin(t) \left(1 + \mu_2 (\sin(t + \mu_3))^2 + 2 \cdot 10^{-3} ((2\pi - t) t)^2\right) \end{bmatrix} \quad (37a)$$

and we denote by $\Omega_{\text{in},\mu}$ the bounded domain such that $\partial\Omega_{\text{in},\mu} = \gamma_\mu([0, 2\pi])$ for all $\mu \in \mathcal{P}$. We further define $\Omega_{\text{box}} = (-2, 2)^2$: note that $\Omega_{\text{in},\mu} \subset \subset \Omega_{\text{box}}$ for all $\mu \in \mathcal{P}$. Then, we introduce the Laplace's problem:

$$-\Delta z_\mu = 0 \quad \text{in } \Omega_\mu, \quad z_\mu|_{\partial\Omega_{\text{in},\mu}} = 1, \quad z_\mu|_{\partial\Omega_{\text{box}}} = 0, \quad (37b)$$

where $\Omega_\mu := \Omega_{\text{box}} \setminus \Omega_{\text{in},\mu}$ is depicted in Figures 8(b) and 8(c) for two values of $\mu \in \mathcal{P}$.

We introduce the reference domain $\Omega = \Omega_{\text{box}} \setminus \Omega_{\text{in}}$, with $\Omega_{\text{in}} = \mathcal{B}_1(\mathbf{0})$: note that Ω is diffeomorphic to Ω_μ for all $\mu \in \mathcal{P}$. Then, given the bijection $\Phi_\mu : \Omega \rightarrow \Omega_\mu$, and the lift R_D such that

$$-\Delta R_D = 0 \quad \text{in } \Omega, \quad R_D|_{\partial\Omega_{\text{in}}} = 1, \quad R_D|_{\partial\Omega_{\text{box}}} = 0, \quad (38a)$$

we define the mapped problem for the lifted solution: find $\tilde{z}_\mu \in \mathcal{X} := H_0^1(\Omega)$ such that

$$\int_{\Omega} \mathbf{K}_\mu \hat{\nabla} (\tilde{z}_\mu + R_D) \cdot \hat{\nabla} v \, dX = 0, \quad \forall v \in \mathcal{X}, \quad (38b)$$

with $\mathbf{K}_\mu := \mathbf{J}_\mu \left(\hat{\nabla} \Phi_\mu \right)^{-1} \left(\hat{\nabla} \Phi_\mu \right)^{-T}$.

RBF maps

We illustrate how to apply RBF approximations to build the mapping Φ_μ for a given $\mu \in \mathcal{P}$. Given an even integer $N_{\text{bnd}} > 0$, the parameterization of $\partial\Omega_{\text{in}}$ $\gamma_{\text{in}} : [0, 1] \rightarrow \partial\Omega_{\text{in}}$, $\gamma_{\text{in}}(t) = [\cos(2\pi t), \sin(2\pi t)]^T$, and the parameterization of $\partial\Omega_{\text{box}}$ $\gamma_{\text{box}} : [0, 1] \rightarrow \partial\Omega_{\text{box}}$, we define the control points

$$\{\mathbf{X}_i\}_{i=1}^{N_{\text{bnd}}} := \left\{ \gamma_{\text{in}}(t^1), \dots, \gamma_{\text{in}}(t^{N_{\text{bnd}}/2}), \gamma_{\text{box}}(t^1), \dots, \gamma_{\text{box}}(t^{N_{\text{bnd}}/2}) \right\},$$

and the displaced control points

$$\{\mathbf{x}_i^\mu\}_{i=1}^{N_{\text{bnd}}} := \left\{ \gamma_{\text{in},\mu}(2\pi t^1), \dots, \gamma_{\text{in},\mu}(2\pi t^{N_{\text{bnd}}/2}), \gamma_{\text{box}}(t^1), \dots, \gamma_{\text{box}}(t^{N_{\text{bnd}}/2}) \right\},$$

where $0 \leq t^1, \dots \leq t^{N_{\text{bnd}}/2} < 1$. Then, we introduce the kernel $\phi : \mathbb{R}^+ \rightarrow \mathbb{R}$, where $\lambda > 0$ is the Kernel width, and the space \mathbb{P}^1 of linear functions from \mathbb{R}^2 to \mathbb{R}^2 . Finally, we define the mapping $\Phi_\mu := \mathbf{p}_\mu + \boldsymbol{\omega}_\mu$ where $(\mathbf{p}_\mu, \boldsymbol{\omega}_\mu)$ is the solution to the optimization problem

$$\min_{(\mathbf{p}, \boldsymbol{\omega}) \in \mathbb{P}^1 \times \mathcal{N}_\phi} \xi \|\boldsymbol{\omega}\|_{\mathcal{N}_\phi}^2 + \sum_{i=1}^{N_{\text{bnd}}} \|\mathbf{p}(\mathbf{X}_i) + \boldsymbol{\omega}(\mathbf{X}_i) - \mathbf{x}_i^\mu\|_2^2. \quad (39)$$

Here, $\xi > 0$ is a regularization parameter, while \mathcal{N}_ϕ is the native Hilbert space associated with the kernel ϕ . We anticipate that in the numerical results we consider the Gaussian kernel with kernel width $\lambda > 0$, $\phi(r) = e^{-\lambda r^2}$ and we resort to hold-out (80%–20%) validation to choose λ and ξ . It is possible to show that the optimal $\boldsymbol{\omega}_\mu$ is of the form $\boldsymbol{\omega}_\mu(\mathbf{X}) = \sum_{i=1}^{N_{\text{bnd}}} \mathbf{a}_i \phi(\|\mathbf{X} - \mathbf{X}_i\|_2)$; as a result, solutions to (39) involve the solution to a linear system of size $d(N_{\text{bnd}} + 1) + d^2$. Note that in [31] the authors consider the pure interpolation problem, which corresponds to taking the limit $\xi \rightarrow 0^+$ in (39) (see [52, Proposition 2.10]).

We observe that Φ_μ defined in (39) is not guaranteed to be bijective for large deformations: this issue is shared by many approaches referenced in the introduction⁷. Furthermore, computational cost scales with $\mathcal{O}(N_{\text{bnd}}^3)$: as N_{bnd} increases, the computational overhead associated with the mapping process might be the dominant online cost.

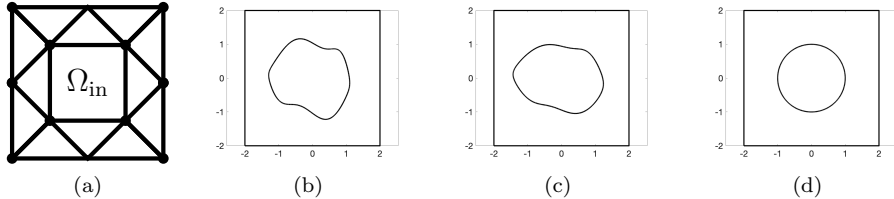


Figure 8: geometry reduction. (a): affine geometry. Black dots denote the user-defined control points associated with the coarse triangulation. (b)-(d): non-affine geometry (section 4.1.2). (b)-(c) show Ω_μ for two values of $\mu \in \mathcal{P}$; (d) shows the reference domain Ω .

4.2 Application of the registration procedure

We consider the parametric function Ψ^{hf} introduced in section 2.1.2 (for the second example we replace Ω by Ω_{box} in Eq. (11)): thanks to this choice, control points can be simply placed on $\partial\Omega_{\text{in},\mu}$. Since, as in the examples of section 3, the conductivity matrix \mathbf{K}_μ and the Jacobian determinant \mathfrak{J}_μ are not expected to be affine, we resort to EIM (cf. Appendix D),

$$\mathbf{K}_\mu \approx \mathbf{K}_\mu^{\text{eim}} := \sum_{q=1}^{Q_a} \Theta_\mu^{q,\kappa} \mathbf{K}_q, \quad \mathfrak{J}_\mu \approx \mathfrak{J}_\mu^{\text{eim}} := \sum_{q=1}^{Q_f} \Theta_\mu^{q,j} \mathfrak{J}_q, \quad (40)$$

⁷ To address this issue, in the related framework of mesh deformation, several authors (see, e.g., [20]) have proposed to resort to nonlinear elasticity extensions: clearly, resorting to a nonlinear extension increases the overall computational cost.

to obtain a parametrically-affine surrogate model. We omit the details.

Some comments are in order. Our approach leads to a non-affine formulation — and thus requires hyper-reduction to achieve online efficiency — for both problems; on the other hand, we observe that the approach exclusively relies on the parameterization of the boundary $\partial\Omega_{\text{in},\mu}$ and can be applied for virtually any choice of the conductivity. We further observe that, unlike the RBF map, the size of the expansion does not depend on the number of control points and — provided that the optimizer for (14) converges — the approach returns a bijection for all μ in the training set $\{\mu^k\}_{k=1}^{n_{\text{train}}} \subset \mathcal{P}$.

4.3 Numerical results

We present below results for the two model problems introduced in section 4.1. Since the focus of this section is geometry reduction, we do not discuss the construction of the ROM for the mapped problems (36) and (38).

4.3.1 Diffusion problem with discontinuous coefficients

We choose $\xi = 10^{-6}$, $\epsilon = 0.1$, $\text{tol}_{\text{POD}} = 10^{-5}$, $\bar{M} = 6$ ($M_{\text{hf}} = 72$); furthermore, we consider the proximity measure (15b) where $\{\mathbf{X}_i\}_{i=1}^{N_{\text{bnd}}}$ is an uniform grid of $\partial\Omega_{\text{in}}$ with $N_{\text{bnd}} = 400$ and $\{\mathbf{x}_i^\mu = \mathbf{X}_i + \mu\}_i$; finally, we consider $n_{\text{train}} = 16^2$ equispaced parameters in \mathcal{P} . For this choice of the parameters, Algorithm 1 returns an affine expansion with $M = 6$ terms.

In Figure 9, we investigate the (linear) complexity of the parametric manifolds associated with (35). In Figure 9(a), we compute the $L^2(\Omega)$ -POD eigenvalues associated with $\{\kappa_{\mu^k}\}_{k=1}^{n_{\text{train}}}$ (unregistered) and $\{\tilde{\kappa}_{\mu^k} = \kappa_{\mu^k} \circ \Phi_{\mu^k}\}_{k=1}^{n_{\text{train}}}$ (registered). We observe that $\lambda_{N=2} \leq 10^{-15} \lambda_{N=1}$ for the registered case: the mapping Φ_μ is able to "fix" the position of the jump discontinuity in the reference configuration⁸. In Figure 9(b), we show the $L^2(\Omega)$ -POD eigenvalues of $\{\mathbf{K}_{\mu^k}\}_{k=1}^{n_{\text{train}}}$ and $\{\mathbf{J}_{\mu^k}\}_{k=1}^{n_{\text{train}}}$. Finally, in Figure 9(c), we show the behavior of the $H^1(\Omega)$ -POD eigenvalues of $\{z_{\mu^k}\}_{k=1}^{n_{\text{train}}}$ (unregistered) and $\{\tilde{z}_{\mu^k}\}_{k=1}^{n_{\text{train}}}$ (registered): even if the mapping is built based on the diffusivity coefficient, it is also effective in improving the linear reducibility of the solution manifold.

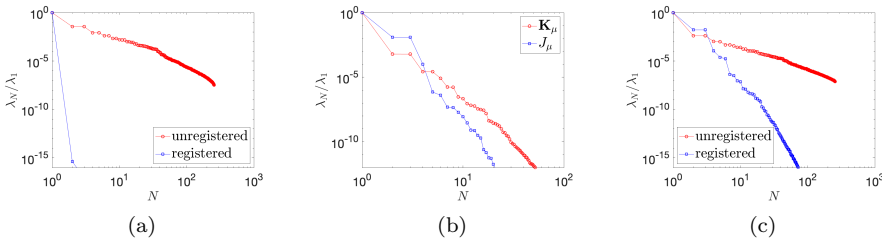


Figure 9: diffusion problem with discontinuous coefficients. Behavior of POD eigenvalues associated with $\{\kappa_{\mu^k}\}_k$ and $\{\tilde{\kappa}_{\mu^k}\}_k$ (Fig. (a)), $\{\mathbf{K}_{\mu^k}\}_k$ and $\{\mathbf{J}_{\mu^k}\}_k$ (Fig. (b)), and $\{z_{\mu^k}\}_k$ and $\{\tilde{z}_{\mu^k}\}_k$ (Fig. (c)).

⁸ More precisely, if we denote by $\{\mathbf{x}_q^{\text{in}}\}_q$ (resp. $\{\mathbf{x}_q^{\text{out}}\}_q$) the FE quadrature points in Ω_{in} (resp. $\Omega \setminus \Omega_{\text{in}}$), we have that $\Phi_\mu(\{\mathbf{x}_q^{\text{in}}\}_q) \subset \Omega_{\text{in},\mu}$ (resp. $\Phi_\mu(\{\mathbf{x}_q^{\text{out}}\}_q) \subset \Omega \setminus \Omega_{\text{in},\mu}$) for all $\mu \in \mathcal{P}$.

In Figure 10, we show the behavior of the mean relative error

$$E_{\text{avg}} := \frac{1}{n_{\text{test}}} \sum_{i=1}^{n_{\text{test}}} \frac{\|\tilde{z}_{\mu^i} - \tilde{z}_{\mu^i}^{\text{eim}}\|_{\star}}{\|\tilde{z}_{\mu^i}\|_{\star}}, \quad \mu^1, \dots, \mu^{n_{\text{test}}} \stackrel{\text{iid}}{\sim} \text{Uniform}(\mathcal{P}), \quad (41)$$

with respect to the tolerance tol_{eim} associated with the choice of Q_a, Q_f in (40) (cf. Appendix D), for $n_{\text{test}} = 20$. Here, $\|\cdot\|_{\star}$ denotes either the $L^2(\Omega)$ norm or the $H^1(\Omega)$ norm:

$$\|w\|_{L^2(\Omega)}^2 = \int_{\Omega} |w|^2 dx, \quad \|w\|_{H^1(\Omega)}^2 = \int_{\Omega} |w|^2 + \|\nabla w\|_2^2 dx.$$

In Figure 10(b), we show the behavior of Q_a, Q_f with respect to tol_{eim} : we observe that the relative H^1 and L^2 errors are less than 10^{-3} , for $Q_a = 19, Q_f = 9$.

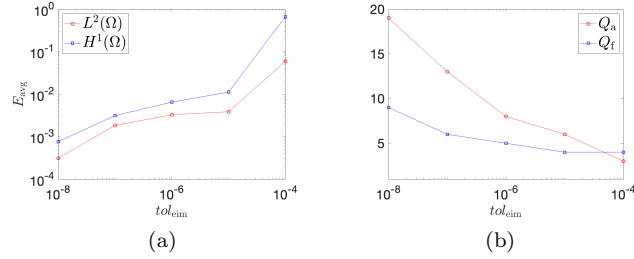


Figure 10: diffusion problem with discontinuous coefficients. (a): behavior of E_{avg} (41) with tol_{eim} ($n_{\text{test}} = 20$). (b): behavior of Q_a, Q_f in (40) with tol_{eim} .

4.3.2 Laplace's equation in parameterized domains

In Figure 11, we compare performance of the RBF map obtained solving (39) with performance of the map obtained solving (14) for several values of M_{hf} , and for a given $\mu \in \mathcal{P}$. Figure 11(a) shows the behavior of $\text{dist}(\Phi_{\mu}(\partial\Omega), \partial\Omega_{\mu})$ with respect to the number of control points N_{bnd} ; Figure 11(b) shows the behavior of the minimum Jacobian determinant over Ω with N_{bnd} . Control points for RBF are chosen on both boundaries $\partial\Omega_{\text{box}}, \partial\Omega_{\text{in}}$ as described in section 4.1.2; on the other hand, in our procedure, in (14), we consider $N_{\text{bnd}} = 10^3$ points on $\partial\Omega_{\text{in}}$. We choose $\epsilon = 0.1$ for all tests, while we observe that higher values of ξ should be considered for small M_{hf} to avoid overfitting: here, we set $\xi = 10^{-4}$ for $M_{\text{hf}} \geq 2 \cdot 4^2$ and $\xi = 10^{-2}$ for $M_{\text{hf}} < 2 \cdot 4^2$. We observe that convergence of RBF maps is relatively slow: this is due to the lack of regularity of $\partial\Omega_{\text{box}}$. We further observe that for small values of $M_{\text{hf}} = N_{\text{bnd}}$ the RBF mapping might be singular. On the other hand, our approach is guaranteed to lead to bijective maps for all choices of M_{hf} .

In Figure 12, we investigate performance of the registration procedure. In this test, we consider $M_{\text{hf}} = 288$, $\xi = 10^{-4}$, $\epsilon = 0.1$, $tol_{\text{POD}} = 10^{-5}$ and we consider uniform grids of $\mathcal{P} \{\mu^k\}_{k=1}^{n_{\text{train}}}$ with $n_{\text{train}} = 4^3, 6^3, 10^3$. "In-sample" box-plots report values of $\max_i \|\Psi_{\mathbf{a}_{\text{hf}}^k}(\mathbf{X}_i) - \mathbf{x}_i^{\mu^k}\|_2$ where \mathbf{a}_{hf}^k is the solution to (14)

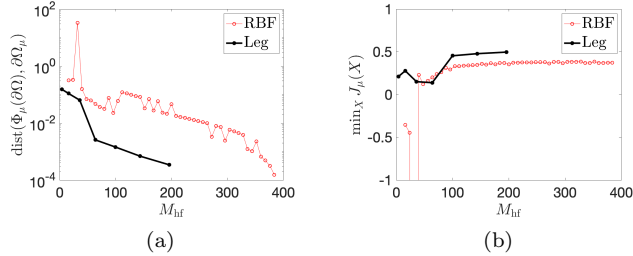


Figure 11: Laplace’s equation in parameterized domain; performance of RBF and Legendre-based mappings for $\mu = [0.1826, 0.2918, 0.4900] \in \mathcal{P}$. (a): behavior of $\text{dist}(\Phi_\mu(\partial\Omega), \partial\Omega_\mu)$ with M_{hf} . (b): behavior of $\min_{\mathbf{X}} \mathfrak{J}_\mu(\mathbf{X})$ with M_{hf} .

for $\mu = \mu^k$; “out-of-sample” boxplots report values of $\{\text{dist}(\Phi_{\mu^i}(\partial\Omega), \partial\Omega_{\mu^i})\}_j$ for $\mu^1, \dots, \mu^{n_{\text{test}}} \stackrel{\text{iid}}{\sim} \text{Uniform}(\mathcal{P})$, $n_{\text{test}} = 50$. In-sample error depends on the choice of the hyper-parameters in (14) and on the choice of the discretization parameter M_{hf} ; on the other hand, out-of-sample error depends on the choice of tol_{POD} and on the number of training points. Interestingly, the value of M is the same (and equal to 7) for all choices of n_{train} .

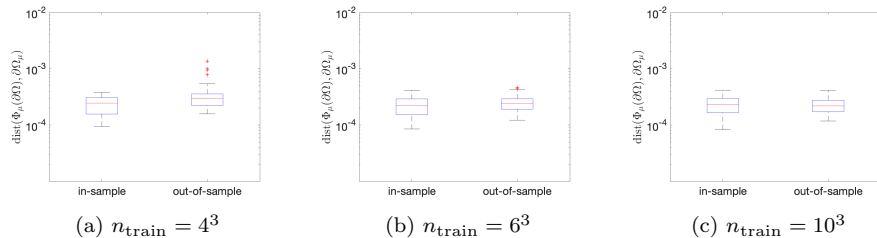


Figure 12: Laplace’s equation in parameterized domain; performance of the registration procedure. Boxplots of in-sample and out-of-sample errors $\text{dist}(\Phi_\mu(\partial\Omega), \partial\Omega_\mu)$ for several training sizes.

Figure 13 replicates the results of Figure 10 for the second model problem. Here, we consider $n_{\text{train}} = 10^3$, $\xi = 10^{-4}$, $M_{\text{hf}} = 288$, $\text{tol}_{\text{POD}} = 10^{-5}$, $\epsilon = 0.1$, and we compute E_{avg} (41) based on $n_{\text{test}} = 50$ parameters. We find that the relative L^2 and H^1 errors are below 10^{-3} for Q_a equal to 17.

5 Summary and discussion

In this work, we proposed a general (i.e., independent of the underlying PDE model) registration procedure, and we applied it to data compression and geometry reduction: in data compression, our registration procedure is used in combination with a linear compression method to devise a *Lagrangian nonlinear compression method*; in geometry reduction, our registration procedure is used to build a parametric mapping from a reference domain to a family of parameterized domains $\{\Omega_\mu\}_{\mu \in \mathcal{P}}$. Several numerical results empirically motivate

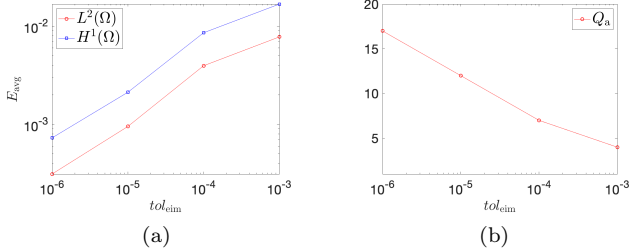


Figure 13: Laplace’s equation in parameterized domain; performance of the registration procedure. (a): behavior of E_{avg} (41) with tol_{eim} ($n_{\text{test}} = 50$). (b): behavior of Q_a in (40) with tol_{eim} .

our proposal. Although the examples considered are rather academic, we believe that our results demonstrate the applicability of our approach to a broad class of relevant problems in science and engineering.

In the future, we wish to extend the approach in several directions. First, in this work, we chose the reference parameter $\bar{\mu}$ that enters in the optimization statement *a priori*; in the future, we wish to develop automatic procedures to adaptively choose $\bar{\mu} \in \mathcal{P}$ or, equivalently, the reference field $\bar{u} \in \mathcal{U}$. Second, in order to tackle problems with more complex parametric behaviors, we also wish to develop partitioning techniques that leverage the use of multiple references. Third, as discussed in section 2, a major limitation of our approach is the need for several offline simulations to train the mapping $\{\Phi_\mu : \mu \in \mathcal{P}\}$. To address this issue, we wish to exploit recent advances in multi-fidelity approaches to reduce the offline computational burden. Alternatively, we wish to assess performance of projection methods to simultaneously learn mapping and solution coefficients during the online stage. Finally, we wish to study the approximation properties of Lagrangian methods based on problem-dependent mappings for a range of parametric problems. Examples 3.1 and 3.2 illustrate the effectivity of Lagrangian mappings for simple one-dimensional problems; in the future, we aim to investigate whether it is possible to prove approximation results for a broader class of problems.

A Notation and implementation details

General notation. We denote by \mathcal{X} the Hilbert ambient space defined over $\Omega \subset \mathbb{R}^d$ endowed with the norm $\|\cdot\| := \sqrt{(\cdot, \cdot)}$; we further denote by $\mathbf{e}_1, \dots, \mathbf{e}_N$ the canonical basis in \mathbb{R}^N and by $\|\cdot\|_2$ the Euclidean norm. Given $A \subset \mathbb{R}^d$, $\mathbb{1}_A : \mathbb{R}^d \rightarrow \{0, 1\}$ is the corresponding indicator function; given the convex set $\mathcal{Z} \subset \mathcal{X}$, $\Pi_{\mathcal{Z}} : \mathcal{X} \rightarrow \mathcal{Z}$ is the orthogonal projection operator onto \mathcal{Z} . The form $\mathcal{G}_\mu : \mathcal{X} \times \mathcal{X} \rightarrow \mathbb{R}$ (cf. (1)) is associated with the parameterized mathematical model, where $\mu = [\mu_1, \dots, \mu_P] \in \mathcal{P} \subset \mathbb{R}^P$ denotes the set of parameters. Finally, $\mathcal{M} := \{z_\mu : \mu \in \mathcal{P}\}$ is the solution manifold.

Mapping. We denote by $\{\Phi_\mu : \mu \in \mathcal{P}\}$ the parametric mapping; we denote by \mathbf{X} (resp. \mathbf{x}) a generic point in the reference (resp. physical) configuration; we use notation $\hat{\nabla}, \nabla, \nabla = \hat{\nabla} \Phi_\mu^{-T} \hat{\nabla}$, to refer to reference and physical gradients;

we denote by $\mathfrak{J}_\mu = \det(\widehat{\nabla} \Phi_\mu)$ the Jacobian determinant; finally, given the field $g \in L^2(\Omega)$, we denote by $\tilde{g}_\mu := g \circ \Phi_\mu$ the corresponding mapped field.

POD. We use the method of snapshots ([51]) to compute POD eigenvalues and eigenvalues. Given the snapshot set $\{u^k\}_{k=1}^{n_{\text{train}}}$ and the inner product (\cdot, \cdot) , we define the Gramian matrix $\mathbf{C} \in \mathbb{R}^{n_{\text{train}}, n_{\text{train}}}$, $\mathbf{C}_{k,k'} = (u^k, u^{k'})$, and we define the POD eigenpairs $\{\lambda_n, \zeta_n\}_{n=1}^{n_{\text{train}}}$ as

$$\mathbf{C} \zeta_n = \lambda_n \zeta_n, \quad \zeta_n := \sum_{k=1}^{n_{\text{train}}} (\zeta_n)_k u^k, \quad n = 1, \dots, n_{\text{train}},$$

with $\lambda_1 \geq \lambda_2 \geq \dots \lambda_{n_{\text{train}}} = 0$. In our implementation, we orthonormalize the modes, that is $\|\zeta_n\| = 1$ for $n = 1, \dots, n_{\text{train}}$.

Mapping procedure. Our implementation of Algorithm 1 takes as input: (i) the reference parameter $\bar{\mu} \in \mathcal{P}$; (ii) the proximity measure \mathfrak{f} (either (15a) or (15b)); (iii) the dataset $\{(\mu^k, u^k)\}_{k=1}^{n_{\text{train}}}$ if $\mathfrak{f} =$ (15a) or $\{(\mathbf{X}_i, \mathbf{x}_i^{\mu^k})\}_{i=1, \dots, N_{\text{bnd}}, k=1, \dots, n_{\text{train}}}$ if $\mathfrak{f} =$ (15b); (iv) the hyper-parameters $\xi, \epsilon, C_{\text{exp}}, \delta$ (cf. (14)) and C_∞ (cf. (16)); (v) the parameterization $\{\Psi_{\mathbf{a}}^{\text{hf}}\}_{\mathbf{a}}$ (cf. (11)-(13)); and (vi) the tolerance tol_{POD} (cf. (21)).

B Proof of Proposition 2.1

B.1 Preliminaries

In view of the proof, we shall introduce notation and recall some standard results and definitions. Let $\Omega \subset \mathbb{R}^d$, $d = 2$ or $d = 3$, be a Lipschitz domain. We denote by $\mathring{\Omega}$ the interior of Ω , we denote by $\partial\Omega$ its boundary, and we denote by $\overline{\Omega} = \Omega \cup \partial\Omega$ the closure; given $\delta > 0$, we also denote by Ω_δ the δ -neighbourhood of Ω , $\Omega_\delta := \{\mathbf{x} \in \mathbb{R}^d : \text{dist}(\mathbf{x}, \Omega) < \delta\}$. Given $\Psi : \Omega \rightarrow \mathbb{R}^d$, we say that Ψ is a homeomorphism (resp. diffeomorphism) from Ω to its image $\Psi(\Omega)$ if Ψ is continuous (resp. differentiable) with continuous (resp. differentiable) inverse; we say that Ω is homeomorphic (resp. diffeomorphic) to V if there exists a homeomorphism (resp. diffeomorphism) from Ω to V .

We denote by \mathcal{O}_Ω the induced (or subspace) topology on Ω , $\mathcal{O}_\Omega := \{A \cap \Omega : A \text{ is open in } \mathbb{R}^d\}$. It is possible to show that the ordered pair $\mathcal{T}_\Omega = (\Omega, \mathcal{O}_\Omega)$ is a topological space. We say that B is open in Ω if $B \in \mathcal{O}_\Omega$; similarly, we say that B is closed in Ω if the complement of B in Ω , $B^c := \Omega \setminus B$, belongs to \mathcal{O}_Ω . We further say that \mathcal{T}_Ω is connected if it cannot be represented as the union of two more disjoint non-empty open subsets; we say that \mathcal{T}_Ω is path-connected if there exists a path joining any two points in Ω ; finally, we say that \mathcal{T}_Ω is simply-connected if \mathcal{T}_Ω is path-connected and every path between two points can be continuously transformed into any other such path while preserving the endpoints. Next three results are key for our discussion. Theorem B.1 is a standard result in Topology that can be found in [33], while Theorem B.2 is known as Hadamard's implicit function theorem and is proven in [26, Chapter 6]. On the other hand, we report the proof of Lemma B.1.

Theorem B.1. *A set A in a topological space \mathcal{T}_Ω is open and closed if and only if $\partial A = \emptyset$. Furthermore, the topological space \mathcal{T}_Ω is connected if and only if the only open and closed sets are the empty set and Ω .*

Theorem B.2. *Let M_1, M_2 be smooth and connected d -dimensional manifolds. Suppose $\Phi : M_1 \rightarrow M_2$ is a C^1 function such that (i) Φ is proper (i.e., for any compact set $K \subset M_2$, $\Phi^{-1}(K)$ is compact in M_1), (ii) the Jacobian matrix of Φ is everywhere invertible, and (iii) M_2 is simply connected. Then, Φ is a homeomorphism (hence globally bijective).*

Lemma B.1. *Let A, B, Ω be connected, open and Lipschitz domains such that $\partial A = \partial B$, and $\overline{A \cup B}$ is strictly contained in $\overline{\Omega}$. Then, $A = B$.*

Proof. Let $C = A \cap B$. Clearly, C is open in A (since it is the intersection of open sets); furthermore, C is closed in A since $\partial A = \partial B$. It thus follows from Theorem B.1 that C is either the empty set or A .

By contradiction, suppose that $C = \emptyset$, and let us define $D = A \cup B$. Since A, B are open, we have $\partial(\overline{A \cup B}) \subset \partial A \cup \partial B = \partial A$. Let $\mathbf{x} \in \partial A$: since (i) $\partial A = \partial B$, (ii) $A \cap B = \emptyset$, and (iii) the boundary of A is smooth, there exists $\epsilon > 0$ such that $\mathcal{B}_\epsilon(\mathbf{x}) \subset \overline{A \cup B}$; therefore, $\mathbf{x} \notin \partial(\overline{A \cup B})$, which implies that $\partial(\overline{A \cup B}) = \emptyset$ and thus (exploiting Theorem B.1) $A \cup B = \Omega$. The latter contradicts the hypothesis that $A \cup B$ is a proper subset of Ω : we can thus conclude that $C = A$.

Exploiting the same argument, we can prove that $C = B$. Thesis follows by applying the transitive property: $A = C, B = C \Rightarrow A = B$. \square

B.2 Proof

We split the proof in four parts.

1. $\Phi(\overline{\Omega}) \subseteq \overline{\Omega}$, $\Omega = \widehat{\Omega} = \{\mathbf{x} \in \mathbb{R}^d : f(\mathbf{x}) < 0\}$. Given $\Omega = \widehat{\Omega} = \{\mathbf{x} \in \mathbb{R}^d : f(\mathbf{x}) < 0\}$ where f is convex, we define $g(\mathbf{X}) = f(\Phi(\mathbf{X}))$. We denote by \mathbf{X}^* a global maximum of g in $\overline{\Omega}$, and we define $\mathbf{x}^* = \Phi(\mathbf{X}^*)$. Since Φ is locally invertible at \mathbf{X}^* , if $\mathbf{X}^* \in \widehat{\Omega}$, we must have that \mathbf{x}^* is a local maximum of f : this is not possible due to the fact that f is convex. As a result, we must have $\mathbf{X}^* \in \partial\Omega$: recalling (iii), we then find

$$\max_{\mathbf{X} \in \overline{\Omega}} f(\Phi(\mathbf{X})) = \max_{\mathbf{X} \in \partial\Omega} f(\Phi(\mathbf{X})) \stackrel{\text{(iii)}}{\leq} \max_{\mathbf{x} \in \partial\Omega} f(\mathbf{x}) = 0,$$

which implies $\Phi(\mathbf{X}) \in \overline{\Omega}$ for all $\mathbf{X} \in \overline{\Omega}$.

2. $\Phi(\overline{\Omega}) = \overline{\Omega}$, $\Omega = \widehat{\Omega}$. Recalling Theorem B.1, we shall simply prove that $\Phi(\overline{\Omega})$ is open and closed in $\overline{\Omega}$.

$\Phi(\overline{\Omega})$ is closed in $\overline{\Omega}$: since Φ is continuous, $\Phi(\overline{\Omega})$ is closed in \mathbb{R}^d ; since $\Phi(\overline{\Omega}) \subseteq \overline{\Omega}$, we then find that $\Phi(\overline{\Omega})$ is closed with respect to the topology of $\overline{\Omega}$.

$\Phi(\overline{\Omega})$ is open in $\overline{\Omega}$. To show this, it suffices to prove that, for any $\mathbf{x} \in \Phi(\overline{\Omega})$, there exists $B \in \mathcal{O}_{\overline{\Omega}}$ such that $B \subset \Phi(\overline{\Omega})$ and $\mathbf{x} \in B$. Given $\mathbf{x} \in \Phi(\overline{\Omega})$, we denote by $\mathbf{X} \in \overline{\Omega}$ a point such that $\mathbf{x} = \Phi(\mathbf{X})$. If \mathbf{X} belongs to the interior of Ω , the proof is trivial; for this reason, we focus below on the case in which $\mathbf{X} \in \partial\Omega$ (and thus $\mathbf{x} \in \partial\Omega$). Exploiting the local inverse-function theorem, there exists $\bar{\eta} > 0$ such that for all $\eta \leq \bar{\eta}$ $\Phi : \mathcal{B}_\eta(\mathbf{X}) \rightarrow A_{\mathbf{x}, \eta}$ is an homeomorphism and $A_{\mathbf{x}, \eta}$ is an open set of \mathbb{R}^d containing $\{\mathbf{x}\}$. Provided that

$$\Phi(\mathcal{B}_\eta(\mathbf{X}) \cap \partial\Omega) = A_{\mathbf{x}, \eta} \cap \partial\Omega, \quad (42)$$

we find that $\Phi(\mathcal{B}_\eta(\mathbf{X}) \cap \bar{\Omega}) = A_{\mathbf{x},\eta} \cap \bar{\Omega}$, $\Phi(\mathcal{B}_\eta(\mathbf{X}) \setminus \bar{\Omega}) = A_{\mathbf{x},\eta} \setminus \bar{\Omega}$. This implies that the set $B := A_{\mathbf{x},\eta} \cap \bar{\Omega}$ is contained in $\Phi(\bar{\Omega})$. Since B is open in $\bar{\Omega}$, we obtain the desired result.

It remains to prove (42). Since Ω is Lipschitz, for sufficiently small values of η , we have that

$$\partial(\mathcal{B}_\eta(\mathbf{X}) \cap \partial\Omega) = \partial\mathcal{B}_\eta(\mathbf{X}) \cap \partial\Omega, \quad \partial(A_{\mathbf{x},\eta} \cap \partial\Omega) = \partial A_{\mathbf{x},\eta} \cap \partial\Omega.$$

Furthermore, these sets are the collection of two distinct points for $\Omega \subset \mathbb{R}^2$, and closed one-dimensional curves for $\Omega \subset \mathbb{R}^3$. Since $\Phi(\partial\Omega) \subset \partial\Omega$, we must have $\Phi(\partial\mathcal{B}_\eta(\mathbf{X}) \cap \partial\Omega) \subset \partial A_{\mathbf{x},\eta} \cap \partial\Omega$; then, since Φ is a local homeomorphism, we conclude that $\Phi(\partial\mathcal{B}_\eta(\mathbf{X}) \cap \partial\Omega) = \partial A_{\mathbf{x},\eta} \cap \partial\Omega$.

We define $A_1 = \Phi(\mathcal{B}_\eta(\mathbf{X}) \cap \partial\Omega)$ and $A_2 = A_{\mathbf{x},\eta} \cap \partial\Omega$. Exploiting once again the fact that Φ is a local homeomorphism and the fact that $\Phi(\partial\mathcal{B}_\eta(\mathbf{X}) \cap \partial\Omega) = \partial A_{\mathbf{x},\eta} \cap \partial\Omega$, we find

$$\partial A_1 = \Phi(\partial\mathcal{B}_\eta(\mathbf{X}) \cap \partial\Omega) = \partial A_{\mathbf{x},\eta} \cap \partial\Omega = \partial A_2.$$

Since A_1, A_2 are connected, open in $\partial\Omega$, Lipschitz, bounded sets with the same boundary, exploiting Lemma B.1, we find $A_1 = A_2$, which is (42).

3. $\Phi(\bar{\Omega}) = \bar{\Omega}$. Let Ψ be a diffeomorphism from $\hat{\Omega}$ to Ω , $\Omega = \Psi(\hat{\Omega})$. Then, we observe that the function $\hat{\Phi} : \hat{\Omega} \rightarrow \hat{\Omega}$, $\hat{\Phi}(\xi) = \Psi^{-1}(\Phi(\Psi(\xi)))$, satisfies the hypotheses (i)-(ii)-(iii) of Proposition 2.1 and thus $\hat{\Phi}(\bar{\hat{\Omega}}) = \bar{\hat{\Omega}}$. Since Ψ and Ψ^{-1} are diffeomorphisms, we obtain

$$\Psi^{-1}(\Phi(\Psi(\bar{\hat{\Omega}}))) = \bar{\hat{\Omega}} \Rightarrow \Phi(\Psi(\bar{\hat{\Omega}})) = \bar{\Omega} \Rightarrow \Phi(\bar{\Omega}) = \bar{\Omega},$$

which is the thesis.

4. $\Phi : \bar{\Omega} \rightarrow \bar{\Omega}$ is bijective. From the third part of the proof, we have that $\Phi(\bar{\Omega}) = \bar{\Omega}$. Since Ω is simply connected, proof follows from Theorem B.2. Note that the condition that Φ is proper follows directly from the fact that Φ is continuous and Ω is bounded.

C DG discretization of (30)

We denote by $\mathbb{P}^\kappa(\hat{\mathcal{D}})$ the space of polynomials of degree at most κ on the triangle $\hat{\mathcal{D}}$ with vertices $(0, 0) - (1, 0) - (0, 1)$; then, we define the broken DG space

$$\mathcal{X} := \left\{ v \in L^2(\Omega) : v|_{\mathcal{D}^k} = \hat{v} \circ \Psi_k^{\text{fe}}, \quad \hat{v} \in \mathbb{P}^\kappa(\hat{\mathcal{D}}), \quad k = 1, \dots, n_{\text{el}} \right\},$$

where $\{\mathcal{D}^k\}_{k=1}^{n_{\text{el}}}$ are the elements of the mesh and $\Psi_k^{\text{fe}} : \mathcal{D}^k \rightarrow \mathcal{D}$ are the local FE mappings. For each edge e of the mesh, we define the positive (resp. negative) normal \mathbf{n}^+ (resp. \mathbf{n}^-); given $w \in \mathcal{X}$ and the mesh edge e , we define the positive and negative limits w^+, w^- and the edge average and jump

$$w^\pm(\mathbf{x}) = \lim_{\epsilon \rightarrow 0^+} w(\mathbf{x} - \epsilon \mathbf{n}^\pm(\mathbf{x})), \quad \{w\} := \frac{w^+ + w^-}{2}, \quad \mathbf{J}w := \mathbf{n}^+ w^+ + \mathbf{n}^- w^-,$$

for all $\mathbf{x} \in e$. If $\mathbf{x} \in e \subset \partial\Omega$, we set $\{w\} := w$ and $\mathbf{J}w := \mathbf{n}w$.

Then, we can introduce the high-fidelity DG discretization of (30): find $z_\mu \in \mathcal{X}$ such that

$$\mathcal{G}_\mu(z_\mu, v) := \mathcal{A}_\mu(z_\mu, v) - \mathcal{F}_\mu(v) = 0, \quad \forall v \in \mathcal{X}, \quad (43a)$$

where

$$\begin{cases} \mathcal{A}_\mu(w, v) = \sum_{k=1}^{n_{\text{el}}} \int_{\mathbb{D}^k} w (\sigma_\mu v - \mathbf{c}_\mu \cdot \nabla v) dx + \int_{\partial\mathbb{D}^k} \mathcal{H}(w, \mathbf{n}) v dx, \\ \mathcal{F}_\mu(w, v) = \sum_{k=1}^{n_{\text{el}}} \int_{\mathbb{D}^k} f_\mu v dx - \int_{\partial\mathbb{D}^k} f_\mu^{\text{ed}} v dx, \end{cases} \quad (43b)$$

Here, $f_\mu^{\text{ed}}(\mathbf{x}) = \delta_{\text{in},\mu} \mathbf{c}_\mu \cdot \mathbf{n} z_{\mathbb{D},\mu}$, where $\delta_{\text{in},\mu}(\mathbf{x}) = 1$ if $\mathbf{x} \in \Gamma_{\text{in},\mu}$ and $\delta_{\text{in},\mu}(\mathbf{x}) = 0$ otherwise, while the flux \mathcal{H} is given by

$$\mathcal{H}(w, \mathbf{n}) := \begin{cases} \mathbf{c}_\mu \cdot \mathbf{n} \{w\} + \frac{1}{2} \tau_\mu \mathbf{n} \cdot (\mathbf{J}w) & \text{on } \partial\mathbb{D}^k \setminus \partial\Omega \\ \mathbf{c}_\mu \cdot \mathbf{n} w \delta_{\text{in},\mu} & \text{on } \partial\mathbb{D}^k \cap \partial\Omega \end{cases} \quad (43c)$$

with $\tau_\mu = |\mathbf{c}_\mu \cdot \mathbf{n}|$.

Then, we introduce

$$\begin{aligned} \mathbf{T}_\mu^{\text{el}} &:= \begin{bmatrix} \sigma_\mu \\ \mathbf{c}_\mu \end{bmatrix}, & \mathbf{T}_\mu^{\text{ed}} &:= (1 - \delta_{\text{in},\mu}) \begin{bmatrix} \mathbf{c}_\mu \cdot \mathbf{n} \\ 0 \end{bmatrix} + \frac{1 - \delta_{\partial\Omega}}{2} \begin{bmatrix} 0 \\ \tau_\mu \end{bmatrix}, \\ A^{\text{el}}(w, v) &:= \begin{bmatrix} w v \\ w \hat{\nabla} v \end{bmatrix}, & A^{\text{ed}}(w, v) &:= \begin{bmatrix} \{w\} v \\ (\mathbf{n} \cdot \mathbf{J}w) v \end{bmatrix}, \end{aligned} \quad (44)$$

where $\delta_{\partial\Omega}(\mathbf{x}) = 1$ if $\mathbf{x} \in \partial\Omega$ and $\delta_{\partial\Omega}(\mathbf{x}) = 0$ otherwise. Exploiting this notation, we can rewrite (43) as (32). Note that the associated mapped problem is of the form (32), provided that we substitute $\mathbf{c}_\mu, \sigma_\mu, f_\mu, z_{\mathbb{D},\mu}$ with the corresponding definitions in (31).

D Empirical Interpolation Method

D.1 Review of the interpolation procedure for scalar fields

We review the Empirical Interpolation Method (EIM, [4]), and we discuss its extension to the approximation of vector-valued fields. Given the Hilbert space \mathcal{W} defined over Ω , the Q -dimensional linear space $\mathcal{W}_Q = \text{span}\{\psi_q\}_{q=1}^Q \subset \mathcal{W}$ and the points $\{\mathbf{x}_q^i\}_{q=1}^Q \subset \overline{\Omega}$, we define the interpolation operator $\mathcal{I}_Q : \mathcal{W} \rightarrow \mathcal{W}_Q$ such that $\mathcal{I}_Q(v)(\mathbf{x}_q^i) = v(\mathbf{x}_q^i)$ for $q = 1, \dots, Q$ for all $v \in \mathcal{W}$. Given the manifold $\mathcal{F} \subset \mathcal{W}$ and an integer $Q > 0$, the objective of EIM is to determine an approximation space \mathcal{Z}_Q and Q points $\{\mathbf{x}_q^i\}_{q=1}^Q$ such that $\mathcal{I}_Q(f)$ accurately approximates f for all $f \in \mathcal{F}$.

Algorithm 3 summarizes the EIM procedure as implemented in our code. The algorithm takes as input snapshots of the manifold $\{f^k\}_{k=1}^{n_{\text{train}}} \subset \mathcal{F}$ and a tolerance $\text{tol}_{\text{eim}} > 0$, and returns the functions $\{\psi_q\}_{q=1}^Q$, the interpolation points $\{\mathbf{x}_q^i\}_{q=1}^Q$ and the matrix $\mathbf{B} \in \mathbb{R}^{Q,Q}$ such that $\mathbf{B}_{q,q'} = \psi_q(\mathbf{x}_{q'}^i)$. It is possible to show that the matrix \mathbf{B} is lower-triangular: for this reason, online computations can be performed in $\mathcal{O}(Q^2)$ flops. Note that in [4] the authors resort to a strong

Greedy procedure to generate \mathcal{Z}_Q , while here (as in several other works including [12]) we resort to POD. A thorough comparison between the two compression strategies is beyond the scope of the present work.

Algorithm 3 Empirical Interpolation Method.

Inputs:	$\{f^k\}_{k=1}^{n_{\text{train}}}$, tol_{eim}
Outputs:	$\{\psi_q\}_{q=1}^Q, \mathbf{B} \in \mathbb{R}^{Q,Q}, \{\mathbf{x}_m^i\}_{m=1}^M$

- 1: Build the POD space $\omega_1, \dots, \omega_Q$ based on the snapshot set $\{f^k\}_{k=1}^{n_{\text{train}}}$; Q is chosen using (21) ($tol_{\text{pod}} = tol_{\text{eim}}$)
- 2: $\mathbf{x}_1^i := \arg \max_{\mathbf{x} \in \bar{\Omega}} |\psi_1(\mathbf{x})|$, $\psi_1 := \frac{1}{\omega_1(\mathbf{x}_1^i)} \omega_1$, $(\mathbf{B})_{1,1} = 1$
- 3: **for** $q = 2, \dots, Q$ **do**
- 4: $r_q = \omega_q - \mathcal{I}_{q-1} \omega_q$
- 5: $\mathbf{x}_q^i := \arg \max_{\mathbf{x} \in \bar{\Omega}} |r_q(\mathbf{x})|$, $\psi_q = \frac{1}{r_q(\mathbf{x}_q^i)} r_q$, $(\mathbf{B})_{q,q} = \psi_q(\mathbf{x}_{q'}^i)$.
- 6: **end for**

Remark D.1. *Oversampling.* Several authors have proposed to consider non-interpolatory extensions of Algorithm 3: these algorithms generate a set of Q_s points $\{\mathbf{x}_q^i\}_{q=1}^{Q_s}$, a basis $\{\psi_q\}_{q=1}^Q$, and the associated system \mathbf{B} , with $Q_s = \mathbf{o}Q$, where $\mathbf{o} > 1$ is the oversampling ratio. We refer to [42] and the references therein for further details; see also [29, Algorithm 2] for a generalization to a broader class of "measurement" functionals.

D.2 Extension to vector-valued fields

The EIM procedure can be extended to vector-valued fields. We present below the non-interpolatory extension of EIM employed in this paper; the same approach has also been employed in [53]. We refer to [55, 36] for two alternatives applicable to vector-valued fields. Given the space $\mathcal{W}_Q = \text{span}\{\omega_q\}_{q=1}^Q \subset \mathcal{W}$ and the points $\{\mathbf{x}_q^i\}_{q=1}^Q \subset \bar{\Omega}$, we define the least-squares approximation operator $\mathcal{I}_Q : \mathcal{W} \rightarrow \mathcal{W}_Q$ such that for all $\mathbf{v} \in \mathcal{W}$

$$\mathcal{I}_Q(\mathbf{v}) := \arg \min_{\omega \in \mathcal{W}_Q} \sum_{q=1}^Q \|\mathbf{v}(\mathbf{x}_q^i) - \omega(\mathbf{x}_q^i)\|_2^2.$$

It is possible to show that \mathcal{I}_M is well-defined if and only if the matrix $\mathbf{B} \in \mathbb{R}^{QD, Q}$,

$$\mathbf{B} = \begin{bmatrix} \omega_1(\mathbf{x}_1^i), & \dots, & \omega_Q(\mathbf{x}_1^i) \\ & \vdots & \\ \omega_1(\mathbf{x}_Q^i), & \dots, & \omega_Q(\mathbf{x}_Q^i) \end{bmatrix} \quad (45a)$$

is full-rank. In this case, we find that \mathcal{I}_Q can be efficiently computed as

$$\mathcal{I}_Q(\mathbf{v}) = \sum_{q=1}^Q (\alpha(\mathbf{v}))_q \omega_q, \quad \alpha(\mathbf{v}) = \mathbf{B}^\dagger \begin{bmatrix} \mathbf{v}(\mathbf{x}_1^i) \\ \vdots \\ \mathbf{v}(\mathbf{x}_Q^i) \end{bmatrix} \quad (45b)$$

for any $\mathbf{v} \in \mathcal{W}$, where $\mathbf{B}^\dagger = (\mathbf{B}^T \mathbf{B})^{-1} \mathbf{B}^T$ denotes the Moore-Penrose pseudo-inverse of \mathbf{B} .

Algorithm 4 summarizes the procedure employed to compute \mathcal{W}_Q , $\{\mathbf{x}_q^i\}_{q=1}^Q$ and the matrix \mathbf{B} . We observe that for scalar fields the procedure reduces to the one outlined in Algorithm 3. We further observe that online computational cost scales with $\mathcal{O}(DQ^2)$, provided that \mathbf{B}^\dagger is computed offline.

Algorithm 4 Empirical Interpolation Method for vector-valued fields.

Inputs:	$\{\mathbf{f}^k\}_{k=1}^{n_{\text{train}}}$, tol_{eim}
Outputs:	$\{\boldsymbol{\omega}_q\}_{q=1}^Q$, $\mathbf{B}^\dagger \in \mathbb{R}^{Q,Q}$, $\{\mathbf{x}_q^i\}_{q=1}^Q$

- 1: Build the POD space $\boldsymbol{\omega}_1, \dots, \boldsymbol{\omega}_Q$ based on the snapshot set $\{\mathbf{f}^k\}_{k=1}^{n_{\text{train}}}$; Q is chosen using (21) ($tol_{\text{pod}} = tol_{\text{eim}}$)
- 2: Set $\mathbf{x}_1^i := \arg \max_{\mathbf{x} \in \bar{\Omega}} \|\boldsymbol{\omega}_1(\mathbf{x})\|_2$, and $\mathbf{B}_{Q=1}$ using (45).
- 3: **for** $q = 2, \dots, Q$ **do**
- 4: $\mathbf{r}_q = \boldsymbol{\omega}_q - \mathcal{I}_{q-1} \boldsymbol{\omega}_q$
- 5: Set $\mathbf{x}_q^i := \arg \max_{\mathbf{x} \in \bar{\Omega}} \|\mathbf{r}_q(\mathbf{x})\|_2$, and update $\mathbf{B}_{Q=q}$ using (45).
- 6: **end for**
- 7: Compute $\mathbf{B}^\dagger = (\mathbf{B}^T \mathbf{B})^{-1} \mathbf{B}$.

Acknowledgments

The author thanks Prof. Angelo Iollo (IMB, Inria), Prof. Pierre Mounoud (IMB), and Prof. Anthony Patera (MIT) for fruitful discussions.

References

- [1] D Amsallem and C Farhat. Interpolation method for adapting reduced-order models and application to aeroelasticity. *AIAA journal*, 46(7):1803–1813, 2008.
- [2] I Babuska and R Lipton. Optimal local approximation spaces for generalized finite element methods with application to multiscale problems. *Multiscale Modeling & Simulation*, 9(1):373–406, 2011.
- [3] J Ballani, DBP Huynh, DJ Knezevic, L Nguyen, and AT Patera. A component-based hybrid reduced basis/finite element method for solid mechanics with local nonlinearities. *Computer Methods in Applied Mechanics and Engineering*, 329:498–531, 2018.
- [4] M Barrault, Y Maday, N C Nguyen, and A T Patera. An empirical interpolation method: application to efficient reduced-basis discretization of partial differential equations. *Comptes Rendus Mathematique*, 339(9):667–672, 2004.
- [5] P Benner, S Gugercin, and K Willcox. A survey of projection-based model reduction methods for parametric dynamical systems. *SIAM review*, 57(4):483–531, 2015.
- [6] M Bergmann, A Ferrero, A Iollo, E Lombardi, A Scardigli, and H Telib. A zonal galerkin-free pod model for incompressible flows. *Journal of Computational Physics*, 352:301–325, 2018.

- [7] G Berkooz, P Holmes, and JL Lumley. The proper orthogonal decomposition in the analysis of turbulent flows. *Annual review of fluid mechanics*, 25(1):539–575, 1993.
- [8] J Brunken, K Smetana, and K Urban. (Parametrized) first order transport equations: realization of optimally stable Petrov–Galerkin methods. *SIAM Journal on Scientific Computing*, 41(1):A592–A621, 2019.
- [9] R H Byrd, M E Hribar, and J Nocedal. An interior point algorithm for large-scale nonlinear programming. *SIAM Journal on Optimization*, 9(4):877–900, 1999.
- [10] N Cagniart, Y Maday, and B Stamm. Model order reduction for problems with large convection effects. In *Contributions to Partial Differential Equations and Applications*, pages 131–150. Springer, 2019.
- [11] K Carlberg. Adaptive h-refinement for reduced-order models. *International Journal for Numerical Methods in Engineering*, 102(5):1192–1210, 2015.
- [12] S Chaturantabut and D C Sorensen. Nonlinear model reduction via discrete empirical interpolation. *SIAM Journal on Scientific Computing*, 32(5):2737–2764, 2010.
- [13] A Cohen and R DeVore. Approximation of high-dimensional parametric PDEs. *Acta Numerica*, 24:1–159, 2015.
- [14] A Cohen and R DeVore. Kolmogorov widths under holomorphic mappings. *IMA Journal of Numerical Analysis*, 36(1):1–12, 2015.
- [15] W Dahmen, C Huang, C Schwab, and G Welper. Adaptive Petrov–Galerkin methods for first order transport equations. *SIAM journal on numerical analysis*, 50(5):2420–2445, 2012.
- [16] A De Boer, MS Van der Schoot, and Hester Bijl. Mesh deformation based on radial basis function interpolation. *Computers & structures*, 85(11-14):784–795, 2007.
- [17] Y Efendiev, E Gildin, and Y Yang. Online adaptive local-global model reduction for flows in heterogeneous porous media. *Computation*, 4(2):22, 2016.
- [18] J L Eftang, M A Grepl, A T Patera, and E M Rønquist. Approximation of parametric derivatives by the empirical interpolation method. *Foundations of computational mathematics*, 13(5):763–787, 2013.
- [19] P Etter and K Carlberg. Online adaptive basis refinement and compression for reduced-order models. *arXiv preprint arXiv:1902.10659*, 2019.
- [20] B Froehle and PO Persson. Nonlinear elasticity for mesh deformation with high-order discontinuous galerkin methods for the navier–stokes equations on deforming domains. In *Spectral and High Order Methods for Partial Differential Equations ICOSAHOM 2014*, pages 73–85. Springer, 2015.
- [21] B Haasdonk. Convergence rates of the pod–greedy method. *ESAIM: Mathematical Modelling and Numerical Analysis*, 47(3):859–873, 2013.
- [22] J S Hesthaven, G Rozza, and B Stamm. *Certified reduced basis methods for parametrized partial differential equations*. Springer, 2016.
- [23] L Iapichino, A Quarteroni, and G Rozza. A reduced basis hybrid method for the coupling of parametrized domains represented by fluidic networks. *Computer Methods in Applied Mechanics and Engineering*, 221:63–82, 2012.
- [24] A Iollo and D Lombardi. Advection modes by optimal mass transfer. *Physical Review E*, 89(2):022923, 2014.
- [25] K Kashima. Nonlinear model reduction by deep autoencoder of noise response data. In *2016 IEEE 55th Conference on Decision and Control (CDC)*, pages 5750–5755. IEEE, 2016.

- [26] S G Krantz and H R Parks. *The implicit function theorem: history, theory, and applications*. Springer Science & Business Media, 2012.
- [27] K Lee and K Carlberg. Model reduction of dynamical systems on nonlinear manifolds using deep convolutional autoencoders. *arXiv preprint arXiv:1812.08373*, 2018.
- [28] Alf Emil Løvgren, Yvon Maday, and Einar M Rønquist. A reduced basis element method for the steady Stokes problem. *ESAIM: Mathematical Modelling and Numerical Analysis*, 40(3):529–552, 2006.
- [29] Y Maday, A T Patera, J D Penn, and M Yano. A parameterized-background data-weak approach to variational data assimilation: formulation, analysis, and application to acoustics. *International Journal for Numerical Methods in Engineering*, 102(5):933–965, 2015.
- [30] A Manzoni and F Negri. Efficient reduction of PDEs defined on domains with variable shape. In *Model Reduction of Parametrized Systems*, pages 183–199. Springer, 2017.
- [31] A Manzoni, A Quarteroni, and G Rozza. Model reduction techniques for fast blood flow simulation in parametrized geometries. *International journal for numerical methods in biomedical engineering*, 28(6-7):604–625, 2012.
- [32] MATLAB. version 9.5 (r2018b), 2018.
- [33] B Mendelson. *Introduction to topology*. Courier Corporation, 1990.
- [34] R Mojgani and M Balajewicz. Arbitrary Lagrangian Eulerian framework for efficient projection-based reduction of convection dominated nonlinear flows. In *APS Division of Fluid Dynamics Meeting Abstracts*, 2017.
- [35] N J Nair and M Balajewicz. Transported snapshot model order reduction approach for parametric, steady-state fluid flows containing parameter-dependent shocks. *International Journal for Numerical Methods in Engineering*, 2018.
- [36] F Negri, A Manzoni, and D Amsallem. Efficient model reduction of parametrized systems by matrix discrete empirical interpolation. *Journal of Computational Physics*, 303:431–454, 2015.
- [37] M Ohlberger and S Rave. Nonlinear reduced basis approximation of parameterized evolution equations via the method of freezing. *Comptes Rendus Mathématique*, 351(23-24):901–906, 2013.
- [38] M Ohlberger and S Rave. Reduced basis methods: success, limitations and future challenges. *arXiv preprint arXiv:1511.02021*, 2015.
- [39] M Ohlberger and F Schindler. Error control for the localized reduced basis multiscale method with adaptive on-line enrichment. *SIAM Journal on Scientific Computing*, 37(6):A2865–A2895, 2015.
- [40] R L Panton. *Incompressible flow*. John Wiley & Sons, 2013.
- [41] B Peherstorfer. Model reduction for transport-dominated problems via online adaptive bases and adaptive sampling. *arXiv preprint arXiv:1812.02094*, 2018.
- [42] B Peherstorfer, Z Drmač, and S Gugercin. Stabilizing discrete empirical interpolation via randomized and deterministic oversampling. *arXiv preprint arXiv:1808.10473*, 2018.
- [43] P-O Persson, J Bonet, and J Peraire. Discontinuous Galerkin solution of the Navier–Stokes equations on deformable domains. *Computer Methods in Applied Mechanics and Engineering*, 198(17-20):1585–1595, 2009.
- [44] A Pinkus. *N-widths in Approximation Theory*, volume 7. Springer Science & Business Media, 2012.

[45] T Poggio, H Mhaskar, L Rosasco, B Miranda, and Q Liao. Why and when can deep-but not shallow-networks avoid the curse of dimensionality: a review. *International Journal of Automation and Computing*, 14(5):503–519, 2017.

[46] A Quarteroni, A Manzoni, and F Negri. *Reduced basis methods for partial differential equations: an introduction*, volume 92. Springer, 2015.

[47] J Reiss, P Schulze, J Sesterhenn, and V Mehrmann. The shifted proper orthogonal decomposition: a mode decomposition for multiple transport phenomena. *SIAM Journal on Scientific Computing*, 40(3):A1322–A1344, 2018.

[48] D Rim and K T Mandli. Model reduction of a parametrized scalar hyperbolic conservation law using displacement interpolation. *arXiv preprint arXiv:1805.05938*, 2018.

[49] D Rim, B Peherstorfer, and Mandli. Nonlinear approximations based on transport modes: A Kolmogorov N-M width and model reduction. in preparation.

[50] G Rozza, DBP Huynh, and AT Patera. Reduced basis approximation and a posteriori error estimation for affinely parametrized elliptic coercive partial differential equations. *Archives of Computational Methods in Engineering*, 15(3):229–275, 2007.

[51] L Sirovich. Turbulence and the dynamics of coherent structures. i. coherent structures. *Quarterly of applied mathematics*, 45(3):561–571, 1987.

[52] T Taddei. An adaptive parametrized-background data-weak approach to variational data assimilation. *ESAIM: Mathematical Modelling and Numerical Analysis*, 51(5):1827–1858, 2017.

[53] T Taddei. An offline/online procedure for dual norm calculations of parameterized functionals: empirical quadrature and empirical test spaces. *arXiv preprint arXiv:1805.08100*, 2018.

[54] T Taddei, S Perotto, and A Quarteroni. Reduced basis techniques for nonlinear conservation laws. *ESAIM: Mathematical Modelling and Numerical Analysis*, 49(3):787–814, 2015.

[55] T Tonn. *Reduced-basis method (RBM) for non-affine elliptic parametrized PDEs*. PhD thesis, PhD thesis, Ulm University, 2011.

[56] C Villani. *Optimal transport: old and new*, volume 338. Springer Science & Business Media, 2008.

[57] S Volkwein. Model reduction using proper orthogonal decomposition. *Lecture Notes, Institute of Mathematics and Scientific Computing, University of Graz*. see <http://www.uni-graz.at/imawww/volkwein/POD.pdf>, 1025, 2011.

[58] G Welper. Interpolation of functions with parameter dependent jumps by transformed snapshots. *SIAM Journal on Scientific Computing*, 39(4):A1225–A1250, 2017.

[59] H Wendland. *Scattered data approximation*, volume 17. Cambridge university press, 2004.

[60] M J Zahr and PO Persson. An optimization based discontinuous Galerkin approach for high-order accurate shock tracking. In *2018 AIAA Aerospace Sciences Meeting*, page 0063, 2018.

[61] R Zimmermann, B Peherstorfer, and K Willcox. Geometric subspace updates with applications to online adaptive nonlinear model reduction. *SIAM Journal on Matrix Analysis and Applications*, 39(1):234–261, 2018.